

Connecting reflective asymmetries in multivariate spatial and spatio-temporal covariances

Drew Yarger*

January 29, 2026

Abstract

In the analysis of multivariate spatial and univariate spatio-temporal data, it is commonly recognized that asymmetric dependence may exist, which can be addressed using an asymmetric (matrix or space-time, respectively) covariance function within a Gaussian process framework. This paper introduces a new paradigm for constructing asymmetric space-time covariances, which we refer to as “reflective asymmetric,” by leveraging recently-introduced models for multivariate spatial data. We first provide new results for reflective asymmetric multivariate spatial models that extends their applicability. We then propose their asymmetric space-time extension, which come from a substantially different perspective than Lagrangian asymmetric space-time covariances. There are fewer parameters in the new models, one controls both the spatial and temporal marginal covariances, and the standard separable model is a special case. In simulation studies and analysis of the frequently-studied Irish wind data, these new models also improve model fit and prediction performance, and they can be easier to estimate. These features indicate broad applicability for improved analysis in environmental and other space-time data.

Keywords: asymmetric dependence, Gaussian processes, multivariate covariances, space-time data, spatial statistics

1 Introduction

Accurately representing spatial dependence structures, which may be quantified through a covariance function, has broad applicability in a variety of environmental applications. Two particular extended settings are multivariate spatial data (Genton and Kleiber, 2015), where multiple spatially-indexed variables are modeled using a matrix-valued covariance function, and spatio-temporal data, where a variable indexed by both space and time is modeled using a space-time covariance function (Chen et al., 2021; Porcu et al., 2021). In these situations, complex dependencies may arise that do not appear in the univariate spatial setting. In particular, there may be

*Department of Statistics, Purdue University, 150 N. University St, West Lafayette, IN 47907, anyarger@purdue.edu

asymmetric dependence between variables (Li and Zhang, 2011) or in space-time (Gneiting et al., 2006). Such asymmetries are physically realistic. For example, the common model for modelling asymmetries in space-time data is the Lagrangian model (Porcu et al., 2021; Salvaña et al., 2023), which can be interpreted as a process evolving with directionality through space over time, like advection through the atmosphere or the ocean following the direction of currents.

In this work, we introduce a new perspective we refer to as “reflective” asymmetries. These asymmetries are enabled by asymmetric cross-covariances in the purely spatial multivariate setting recently introduced in Yarger et al. (2026). These cross-covariances (describing the covariance between two spatial variables) result from multiplication in the spectral domain of $-\text{i}\text{sign}(\langle \mathbf{x}, \tilde{\mathbf{x}} \rangle)$ to the spectral density $f(\mathbf{x})$ of a spatial covariance, where $\mathbf{x} \in \mathbb{R}^d$ is the spatial frequency ($d \in \{1, 2, 3, \dots\}$), $\tilde{\mathbf{x}} \in \mathbb{R}^d$ is a unit-vector directional parameter, i is the imaginary unit, $\text{sign}(z)$ is the sign function, and $\langle \cdot, \cdot \rangle$ is the Euclidean inner product in \mathbb{R}^d . The resulting term in the cross-covariance is an odd function, reflected across the origin, which motivates the “reflective” terminology. We first introduce new spatial cross-covariances of this type, which previously had established closed forms only for $d = 1$ but are extended here to any dimension d for squared-exponential and Cauchy covariances. The main focus of this work, however, is applying such constructions to the univariate space-time setting.

The new space-time models are defined by introducing a term that multiplies $\text{sign}(\langle \mathbf{x}, \tilde{\mathbf{x}} \rangle)\text{sign}(\eta)$ onto a spectral density $f(\mathbf{x}, \eta)$ of a symmetric space-time covariance, where $\eta \in \mathbb{R}$ is the temporal frequency. In many cases, the new asymmetric parts of the space-time covariance are constructed from asymmetric spatial cross-covariances, connecting the two settings. This construction results in a two-term decomposition of the space-time covariance function into a symmetric space-time covariance function and a term that introduces asymmetry. These models include some asymmetric versions of Gneiting-type nonseparable space-time covariances (Gneiting, 2002), which are generally symmetric but nonseparable.

These models have some conceptual advantages over the Lagrangian model. The nontrivial symmetric and separable space-time model is a special case of the reflective asymmetric model, which is not the case for the Lagrangian model. Thus, one may evaluate the presence of asymmetric dependence through a likelihood ratio test. Furthermore, one maintains control of both the marginal spatial and temporal covariance functions, while independent control of the temporal covariance function is not available for the Lagrangian model. Control of the marginal covariances (and their spectral density) has implications for the asymptotic behavior of parameter estimation and prediction (Section 5.2, Faouzi et al., 2025). The reflective asymmetric model also has fewer parameters than the full Lagrangian model, providing model parsimony, especially for larger spatial dimension d .

We also propose approaches for unconditional simulation, nonstationary and anisotropic construction, and computational implementation for large space-time data through Vecchia’s approximation (Guinness et al., 2021). In multivariate spatial and univariate space-time simulation studies, we find that using asymmetric models can improve model fit when the true covariance is asym-

metric. We establish that the new models are substantially different than the Lagrangian model, where neither can perform as well when the other is the true model.

These models are also evaluated in an analysis of the Irish wind data of Haslett and Raftery (1989), which has been frequently used as a benchmark dataset (Gneiting et al., 2006; Ma, 2025). We consider five variations of the new asymmetric models with different marginal covariances. In general, the asymmetric models outperform the symmetric models in terms of model selection criteria. Depending on the covariance function used, the reflective asymmetric covariances can provide improved model fit and faster likelihood estimation than the Lagrangian model.

These developments are presented in the following. In Section 2, we introduce relevant background in more detail. In Section 3, we review and introduce new spatial cross-covariance functions with reflective asymmetries. In Section 4, the new univariate space-time covariances are introduced. In Section 5, we discuss efficient simulation and computation. Section 6 presents the simulation studies. Section 7 presents a comprehensive analysis of the Irish wind data. We conclude in Section 8.

2 Background and literature

The basic univariate spatial setting considers a random field $\{Y(\mathbf{s}), \mathbf{s} \in \mathbb{R}^d\}$ for $d \in \{1, 2, 3, \dots\}$. Throughout much of the exposition, we will assume second-order stationarity, where the mean and covariance do not depend on \mathbf{s} : $\mathbb{E}\{Y(\mathbf{s})\} = \mu$ and

$$\text{Cov}\{Y(\mathbf{s}), Y(\mathbf{s} + \mathbf{h})\} = \mathbb{E}\{(Y(\mathbf{s}) - \mu)(Y(\mathbf{s} + \mathbf{h}) - \mu)\} = C(\mathbf{h}).$$

Here $\mathbf{h} \in \mathbb{R}^d$ is a lag; in the case $d = 1$, scalar operations (for example, $\|\mathbf{h}\|^2 = h^2$) may be used. Our primary interest is the covariance function $C(\mathbf{h})$, which requires $C(\mathbf{0}) \geq 0$ and symmetry $C(\mathbf{h}) = C(-\mathbf{h})$, including further conditions for validity. We will assume that $\mu = 0$ and similarly for a multivariate mean below. Throughout, covariance functions depend on parameters $\boldsymbol{\theta}$, but we suppress this notation for simplicity.

We will next provide background on multivariate and space-time models.

2.1 Multivariate spatial models

Let $\{\mathbf{Y}(\mathbf{s}) \in \mathbb{R}^p, \mathbf{s} \in \mathbb{R}^d\}$ be a multivariate random field which now has a $p \times p$ matrix-valued covariance function $\mathbf{C}(\mathbf{h}) = \mathbb{E}\{(\mathbf{Y}(\mathbf{s}) - \boldsymbol{\mu})(\mathbf{Y}(\mathbf{s} + \mathbf{h}) - \boldsymbol{\mu})^\top\} = [C_{jk}(\mathbf{h})]_{j,k=1}^p$, and $\boldsymbol{\mu} = \mathbb{E}\{\mathbf{Y}(\mathbf{s})\}$. Let $\{Y_j(\mathbf{s}), \mathbf{s} \in \mathbb{R}^d\}$ be the j -th entry of $\{\mathbf{Y}(\mathbf{s})\}$. The diagonals of $\mathbf{C}(\mathbf{h})$ are the covariance functions of the processes, while the off-diagonal indicate the dependence between processes j and k at different spatial lags, termed cross-covariances. See Genton and Kleiber (2015) for a review.

Theorem 1 (Simplified multivariate Bochner). The matrix-valued stationary covariance $\mathbf{C}(\mathbf{h})$ is

valid (positive-definite) if we have spectral representation

$$\mathbf{C}(\mathbf{h}) = \int_{\mathbb{R}^d} \exp(\mathbf{i}\langle \mathbf{h}, \mathbf{x} \rangle) \mathbf{f}(\mathbf{x}) d\mathbf{x} = \left[\int_{\mathbb{R}^d} \exp(\mathbf{i}\langle \mathbf{h}, \mathbf{x} \rangle) f_{jk}(\mathbf{x}) d\mathbf{x} \right]_{j,k=1}^p,$$

and the $p \times p$ matrix $\mathbf{f}(\mathbf{x})$ is Hermitian (satisfying $f_{jk}(\mathbf{x}) = \overline{f_{jk}(-\mathbf{x})} = \overline{f_{kj}(\mathbf{x})}$, where \overline{z} represents the conjugate of z) and positive-definite for all \mathbf{x} .

See [Gneiting et al. \(2010\)](#), or [Yarger et al. \(2026\)](#) for a more technical statement, where the careful use of spectral measures makes the statement if and only if.

Many of the cross-covariances proposed have been proportional to a covariance function $C^*(\mathbf{h}; \boldsymbol{\theta}_j)$. For example, if $C_{jj}(\mathbf{h}) = C^*(\mathbf{h}; \boldsymbol{\theta}_j)$ and $C_{kk}(\mathbf{h}) = C^*(\mathbf{h}; \boldsymbol{\theta}_k)$, then one might use $C_{jk}(\mathbf{h}) = \rho_{jk}C^*(\mathbf{h}; \boldsymbol{\theta}_{jk})$ for some set of parameters $\boldsymbol{\theta}_{jk}$ and $\rho_{jk} \in [-1, 1]$, which may need to be restricted further. At times, ensuring the validity of such multivariate models is quite nontrivial ([Gneiting et al., 2010](#); [Apanasovich et al., 2012](#); [Emery et al., 2022](#)). In general, cross-covariances, unlike spatial covariances, may be asymmetric, where $C_{jk}(\mathbf{h}) \neq C_{jk}(-\mathbf{h})$ for $j \neq k$, which we discuss here.

Definition 1 (Multivariate symmetry). A stationary multivariate covariance $\mathbf{C}(\mathbf{h})$ is symmetric if $\mathbf{C}(\mathbf{h}) = \mathbf{C}(-\mathbf{h})$ for all $\mathbf{h} \in \mathbb{R}^d$.

Constructions based on $C_{jk}(\mathbf{h}) = \rho_{jk}C^*(\mathbf{h}; \boldsymbol{\theta}_{jk})$ are inherently symmetric as $C^*(\mathbf{h}; \boldsymbol{\theta}_{jk})$ is proportional to a covariance function. If the spectral density exists, symmetry holds if and only if $\mathbf{f}(\mathbf{x})$ is real-valued for all $\mathbf{x} \in \mathbb{R}^d$ ([Section 2.1](#), [Yarger et al., 2026](#)). Most asymmetric cross-covariances $C_{jk}(\mathbf{h})$ are based on shifts, where $C_{jk}(\mathbf{h}) = \rho_{jk}C^*(\mathbf{h} - \mathbf{v}_{jk}; \boldsymbol{\theta}_{jk})$ for a covariance $C^*(\mathbf{h}; \boldsymbol{\theta}_{jk})$ and a shift vector $\mathbf{v}_{jk} \in \mathbb{R}^d$ ([Li and Zhang, 2011](#); [Vu et al., 2022](#); [Mu et al., 2025](#)). This shift corresponds to a multiplication of $\exp\{-\mathbf{i}\langle \mathbf{v}_{jk}, \mathbf{x} \rangle\}$ on the entry $f_{jk}(\mathbf{x})$ in the spectral domain. Recently, [Yarger et al. \(2026\)](#) introduced asymmetric multivariate covariances using another approach with the spectral density, which is the main topic of [Section 3](#).

2.2 Univariate spatio-temporal models

We now review some key definitions and covariance models in spatio-temporal statistics. We assume here that a covariance function $C(\mathbf{h}, u)$ of a space-time process $\{Y(\mathbf{s}, t) \in \mathbb{R}; \mathbf{s} \in \mathbb{R}^d, t \in \mathbb{R}\}$ is finite and covariance stationary, in that the covariance $C(\mathbf{h}, u) = \text{Cov}\{Y(\mathbf{s}, t), Y(\mathbf{s} + \mathbf{h}, t + u)\} < \infty$ does not depend on \mathbf{s} or t . We focus on a few properties of space-time covariances, where more information can be found in [Gneiting et al. \(2006\)](#); [Porcu et al. \(2021\)](#); [Chen et al. \(2021\)](#).

Theorem 2 (Simplified Bochner, space-time covariances). Define a spectral density $f(\mathbf{x}, \eta)$ that is integrable and satisfies $f(-\mathbf{x}, -\eta) = f(\mathbf{x}, \eta)$ and nonnegativity $f(\mathbf{x}, \eta) \geq 0$ for all $\mathbf{x} \in \mathbb{R}^d$ and $\eta \in \mathbb{R}$. Then the following is a valid space-time covariance on $\mathbb{R}^d \times \mathbb{R}$:

$$C(\mathbf{h}, u) = \int_{\mathbb{R}} \int_{\mathbb{R}^d} \exp\{\mathbf{i}(\langle \mathbf{h}, \mathbf{x} \rangle + u\eta)\} f(\mathbf{x}, \eta) d\mathbf{x} d\eta.$$

We propose asymmetric covariance models through the spectral density $f(\mathbf{x}, \eta)$. One simplified construction of space-time models is through separability.

Definition 2 (Separability). A space-time stationary covariance $C(\mathbf{h}, u)$ is called separable if a decomposition $C(\mathbf{h}, u) = C_s(\mathbf{h})C_t(u)$ exists for all $\mathbf{h} \in \mathbb{R}^d$ and $u \in \mathbb{R}$.

In general, separability is often considered to be restrictive (Chen et al., 2021; De Iaco and Posa, 2013). If a covariance is not separable, then we say it is nonseparable. A common separability measure is $R(\mathbf{h}, u) = C(\mathbf{h}, u)C(\mathbf{0}, 0) - C(\mathbf{h}, 0)C(\mathbf{0}, u)$, where $R(\mathbf{h}, u) = 0$ for all \mathbf{h} and u corresponds to separability. Positive nonseparability occurs if $R(\mathbf{h}, u) > 0$ for some \mathbf{h} and u and negative nonseparability if $R(\mathbf{h}, u) < 0$ (De Iaco and Posa, 2013). We refer to $C(\mathbf{h}, 0)$ and $C(\mathbf{0}, u)$ as the marginal spatial and temporal covariance functions, respectively.

We now introduce a celebrated nonseparable and symmetric class of space-time covariances called the Gneiting class (Gneiting, 2002), which built upon results in Cressie and Huang (1999). We principally use the form of the wider “extended” class discussed in Allard et al. (2025) with a separability parameter $b \in [0, 1]$, where $b = 0$ corresponds to separability. With the additional parameter $\delta > 0$, and letting $\tau = b/2 + \delta > b/2$, consider the covariance

$$C(\mathbf{h}, u) = \frac{\sigma}{(\gamma(u) + 1)^\tau} \varphi \left\{ \frac{\|\mathbf{h}\|^2}{(\gamma(u) + 1)^b} \right\}, \quad (1)$$

where $\gamma(u)$ is a continuous variogram on \mathbb{R} and $\varphi(r)$ is a completely monotone function on $[0, \infty)$. Gneiting covariances only introduce positive nonseparability (De Iaco and Posa, 2013). We next discuss symmetry and asymmetry in space-time covariances, the principal characteristic motivating this paper.

Definition 3 (Full symmetry). A space-time covariance $C(\mathbf{h}, u)$ is fully symmetric, if, for all $\mathbf{h} \in \mathbb{R}^d$ and $u \in \mathbb{R}$, $C(\mathbf{h}, u) = C(-\mathbf{h}, u) = C(\mathbf{h}, -u) = C(-\mathbf{h}, -u)$.

If a covariance is not fully symmetric, then we say it is asymmetric, though $C(\mathbf{h}, u) = C(-\mathbf{h}, -u)$ must be satisfied. All covariances that are separable are also fully symmetric (Gneiting et al., 2006). Park and Fuentes (2008) propose statistical tests for symmetry in space-time data. Park and Fuentes (2008) also define axial symmetry with respect to the k -th spatial dimension, as defined here.

Definition 4 (Axial symmetry). A space-time covariance is axially symmetric in space with respect to the k -th dimension if $C(\mathbf{h}, u) = C(\mathbf{h}^*, u)$ for any pairs $(\mathbf{h}, \mathbf{h}^*)$ whose entries satisfy $h_j = h_j^*$ for all $j \neq k$ and $h_k = -h_k^*$.

The most-commonly referred-to class of asymmetric space-time covariances are Lagrangian covariances (Gneiting et al., 2006; Salvaña et al., 2023; Porcu et al., 2021; Chen et al., 2021; Fonseca and Steel, 2011; Ezzat et al., 2018). In this case, one takes $C(\mathbf{h}, u) = \mathbb{E}_{\mathbf{V}} \{C_s(\mathbf{h} - u\mathbf{V})\}$, where $C_s(\mathbf{h})$ is a purely spatial covariance function, \mathbf{V} is a random vector in \mathbb{R}^d , and the expectation is

taken with respect to \mathbf{V} . An advantage of this model is the interpretability. For example, when $Y(\mathbf{s}, t)$ represents an atmospheric variable, the distribution of \mathbf{V} could represent the wind direction and speed, transporting the variable through space over time.

The expectation can be simplified when using the squared-exponential covariance with $C_{\mathbf{s}}(\mathbf{h}) = \sigma \exp(-a_{\mathbf{s}}^2 \|\mathbf{h}\|^2)$, where $\sigma > 0$ is a variance parameter and $a_{\mathbf{s}} > 0$ is an inverse range parameter. If we also have $\mathbf{V} \sim \mathcal{N}(\boldsymbol{\mu}_{\mathbf{V}}, \boldsymbol{\Sigma}_{\mathbf{V}})$, where $\mathcal{N}(\cdot, \cdot)$ is the multivariate normal distribution, the Lagrangian covariance is

$$C(\mathbf{h}, u) = \sigma \frac{1}{|I_d + 2a_{\mathbf{s}}^2 u^2 \boldsymbol{\Sigma}_{\mathbf{V}}|^{\frac{1}{2}}} \exp \left\{ -a_{\mathbf{s}}^2 (\mathbf{h} - u \boldsymbol{\mu}_{\mathbf{V}})^{\top} (I_d + 2a_{\mathbf{s}}^2 u^2 \boldsymbol{\Sigma}_{\mathbf{V}})^{-1} (\mathbf{h} - u \boldsymbol{\mu}_{\mathbf{V}}) \right\}, \quad (2)$$

where I_d is the $d \times d$ identity matrix and $|\boldsymbol{\Sigma}|$ is the determinant of $\boldsymbol{\Sigma}$ (Schlather, 2010; Salvaña and Genton, 2021; Salvaña et al., 2023; Zhang et al., 2024). The covariance is asymmetric if $\boldsymbol{\mu}_{\mathbf{V}} \neq \mathbf{0}$ (Salvaña and Genton, 2021). Similar representations exist for other scale-mixture covariances (Zhang et al., 2024; Schlather, 2010; Ma, 2025). The marginal covariances are $C(\mathbf{h}, 0) = \sigma \exp(-a_{\mathbf{s}}^2 \|\mathbf{h}\|^2)$ and $C(\mathbf{0}, u) = \sigma |I_d + 2a_{\mathbf{s}}^2 u^2 \boldsymbol{\Sigma}_{\mathbf{V}}|^{-1/2} \exp \left\{ a_{\mathbf{s}}^2 u^2 \boldsymbol{\mu}_{\mathbf{V}}^{\top} (I_d + 2a_{\mathbf{s}}^2 u^2 \boldsymbol{\Sigma}_{\mathbf{V}})^{-1} \boldsymbol{\mu}_{\mathbf{V}} \right\}$, with the temporal marginal covariance affected by the spatial covariance function. Theoretical asymptotic parameter estimation and prediction results typically require appropriate control of both marginal spectral densities (Section 5.2, Faouzi et al., 2025). The only separable Lagrangian covariance takes $\mathbf{V} = \mathbf{0}$, a trivial case where $C(\mathbf{0}, u)$ is constant in u . The Lagrangian model has $1 + 1 + d + d(d+1)/2$ parameters through $(\sigma, a_{\mathbf{s}}, \boldsymbol{\mu}_{\mathbf{V}}, \boldsymbol{\Sigma}_{\mathbf{V}})$, respectively. Salvaña and Genton (2021) show that some Gneiting models correspond to Lagrangian models when $\boldsymbol{\mu}_{\mathbf{V}} = \mathbf{0}$ and $\boldsymbol{\Sigma}_{\mathbf{V}} = cI_d$.

Other asymmetric space-time covariances have also been introduced. The approach in Section 5 of Stein (2005) is most similar to ours by using the spectral density

$$f(\mathbf{x}, \eta) = f^*(\|\mathbf{x}\|, |\eta|) (1 + \langle \mathbf{x}, \tilde{\mathbf{x}} \rangle \eta + \|\mathbf{x}\|^2 + \eta^2),$$

where $f^*(\|\mathbf{x}\|, |\eta|)$ is the spectral density of a symmetric space-time covariance and $\tilde{\mathbf{x}} \in \mathbb{R}^d$. However, additional requirements are needed for validity. Horrell and Stein (2017) defines a half-spectral approach, where one of the two integrals in Bochner's representation have been evaluated. In particular, asymmetry is introduced by $C(\mathbf{h}, u) = \int_{\mathbb{R}} \exp(i\eta u) \exp\{i\phi(\eta) \langle \tilde{\mathbf{x}}, \mathbf{h} \rangle\} f_{\text{half}}(\eta; \mathbf{h}) d\eta$ for some odd function $\phi(\eta)$, with $\phi(\eta) = 0$ as the symmetric case. Finally, Wu (2021) and Zhang and Zhang (2017) describe an approach for asymmetry through scale-mixtures with space-time interaction. However, covariances are only available through an infinite series.

Approaches to combine Lagrangian and Gneiting covariances have also been considered, aiming to give flexible control over both asymmetry and nonseparability. These primarily consist of convex combinations (Gneiting et al., 2006; Chen et al., 2021), where $C(\mathbf{h}, u) = \sigma(1 - \lambda)C_{NS}(\mathbf{h}, u) + \sigma\lambda C_{LA}(\mathbf{h}, u)$ for $\lambda \in (0, 1)$, $C_{NS}(\mathbf{h}, u)$ is Gneiting and $C_{LA}(\mathbf{h}, u)$ is Lagrangian. However, there is not necessarily harmony between the covariance functions, as often $C_{LA}(\mathbf{h}, u)$ is compact unlike $C_{NS}(\mathbf{h}, u)$, and they may imply different origin behavior of the covariance.

3 Previously-established and new asymmetric cross-covariances

We next provide background and new results on asymmetric cross-covariances. In [Yarger et al. \(2026\)](#), cross-covariance functions were introduced of the form

$$C_{jk}(\mathbf{h}) = \int_{\mathbb{R}^d} \exp(\mathbf{i}\langle \mathbf{h}, \mathbf{x} \rangle) \{ \Re(\sigma_{jk}) - \mathbf{i}\text{sign}(\langle \mathbf{x}, \tilde{\mathbf{x}} \rangle) \Im(\sigma_{jk}) \} \sqrt{f_j(\mathbf{x})f_k(\mathbf{x})} d\mathbf{x},$$

where $\{f_j(\mathbf{x})\}$ are the individual spectral densities of each process, $\Re(z)$ and $\Im(z)$ the real and imaginary parts of z , respectively, $\boldsymbol{\sigma} = [\sigma_{jk}]_{j,k=1}^p$ is a positive definite, Hermitian matrix with potentially complex entries on the off-diagonal, and $\tilde{\mathbf{x}}$ is a unit vector of length d . We will also use \Re and \Im as superscripts to refer to functions involving symmetric or asymmetric parts of a cross-covariance or space-time covariance. For $d = 1$, we generally take $\tilde{\mathbf{x}} = \tilde{x} = 1$, and we can also represent the cross-covariance $C_{jk}(h) = 2 \int_0^\infty \{\cos(hx)\Re(\sigma_{jk}) + \sin(hx)\Im(\sigma_{jk})\} \sqrt{f_j(x)f_k(x)} dx$. For general d , this leads to a decomposition

$$C_{jk}(\mathbf{h}) = \Re(\sigma_{jk})C_{jk}^{\Re}(\mathbf{h}) + \Im(\sigma_{jk})C_{jk}^{\Im}(\mathbf{h}), \quad (3)$$

where $C_{jk}^{\Re}(\mathbf{h})$ is symmetric, and $C_{jk}^{\Im}(\mathbf{h})$ introduces asymmetry when $\Im(\sigma_{jk}) \neq 0$.

When $d = 1$, $C_{jk}^{\Im}(h)$ will be proportional to the Hilbert transform of $C_{jk}^{\Re}(h)$ ([King, 2009](#)), which corresponds to the Fourier multiplier $-\mathbf{i}\text{sign}(x)$. Thus, if $C_{jk}^{\Re}(h) = C_{jk}^{\Re}(-h)$ is an even function, then $C_{jk}^{\Im}(h) = -C_{jk}^{\Im}(-h)$ will be an odd function, and many such closed forms for $C_{jk}^{\Im}(h)$ can be found using tables in [King \(2009\)](#). For $d > 1$, the Fourier multiplier $-\mathbf{i}\text{sign}(\langle \mathbf{x}, \tilde{\mathbf{x}} \rangle)$ has been studied under a variety of names, including the directional Hilbert transform ([King 2009, 487, 571](#) of [García-Cuerva 1985](#)), the Hilbert transform in multiple dimensions (172 of [Granolund and Knutsson, 2013](#)), and the partial Hilbert transform ([Felsberg and Sommer, 2002](#)).

We next concretely present $C_{jk}^{\Im}(\mathbf{h})$ for some covariances. In these forms, we implicitly assume that $f_j(\mathbf{x}) = f_k(\mathbf{x})$, but the full versions are given in [Appendix A.1](#). Throughout, proofs for propositions are also presented in [Appendix C](#).

3.1 Squared-exponential covariance

As mentioned in Section 7.6 of [Yarger et al. \(2026\)](#), the squared-exponential covariance in $d = 1$, $C_{jk}^{\Re}(h) = \exp(-a^2h^2)$ where $a > 0$ is an inverse range parameter, has $C_{jk}^{\Im}(h) = (2/\sqrt{\pi})D_+(ah)$, where $D_+(z)$ is Dawson's function, represented by $D_+(z) = (1/2)\int_0^\infty \exp(-t^2/4) \sin(zt) dt = (\sqrt{\pi}/2) \exp(-z^2) \text{erfi}(z)$, where $\text{erfi}(z)$ is the imaginary error function. See, for example, Section 7 (7.2.5, 7.5.1) of [DLMF](#). This result is Hilbert transform numbered (3.5) in the tables of [King \(2009\)](#). We next introduce the novel extended result for general d .

Proposition 1. Consider the cross-covariance $C_{jk}^{\Re}(\mathbf{h}) = \exp(-a^2\|\mathbf{h}\|^2)$ where $\mathbf{h} \in \mathbb{R}^d$. The asymmetric part corresponding to the $-\mathbf{i}\text{sign}(\langle \mathbf{x}, \tilde{\mathbf{x}} \rangle)$ Fourier multiplier is

$$C_{jk}^{\Im}(\mathbf{h}) = \exp(-a^2\|\mathbf{h}\|^2) \text{erfi}(a\langle \mathbf{h}, \tilde{\mathbf{x}} \rangle).$$

In the top-left facet of Figure 1, we plot an example of $C_{jk}^{\Im}(\mathbf{h})$ for $d = 2$.

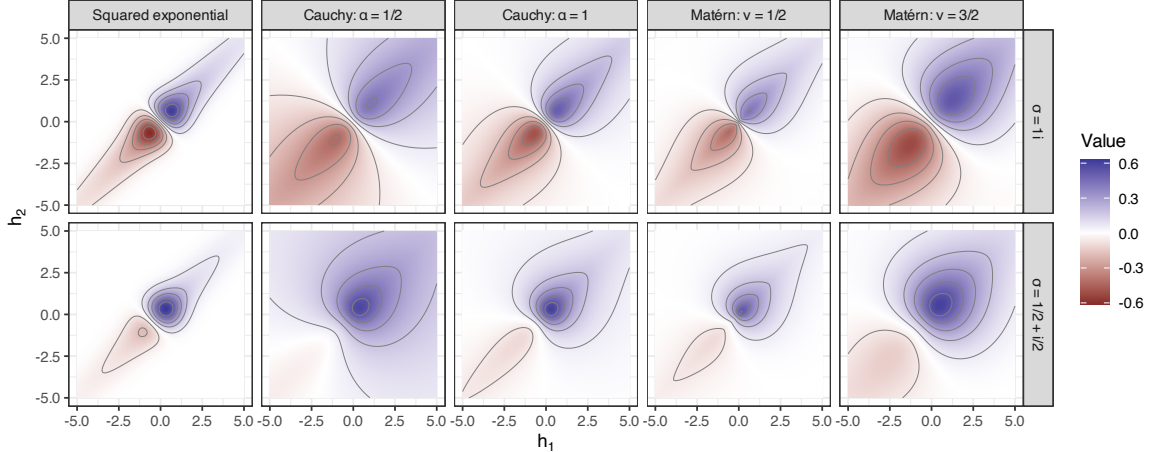


Figure 1: Squared-exponential, Cauchy, and Matérn cross-covariances $\Re(\sigma_{jk})C_{jk}^{\Re}(\mathbf{h}) + \Im(\sigma_{jk})C_{jk}^{\Im}(\mathbf{h})$ in $d = 2$. In all cases, we take $a = 1$, $\tilde{\mathbf{x}} = (1, 1)^{\top}/\sqrt{2}$. On the top row, we plot $C_{jk}^{\Im}(\mathbf{h})$, while the bottom row takes $\Re(\sigma_{jk}) = \Im(\sigma_{jk}) = 1/2$.

This representation for the squared-exponential form provides a basis to find additional asymmetric cross-covariances for other covariance functions through Schoenberg's theorem (Allard et al., 2025). In particular, suppose $C(\mathbf{h}) = \sigma \int_0^\infty \exp(-v\|\mathbf{h}\|^2) g(v)dv$ where $g(v)$ is a nonnegative mixing density. Then $C(\mathbf{h})$ is a valid covariance function for any d , and we say that $C(\mathbf{h})$ has a normal Gaussian scale-mixture representation (Allard et al., 2025). This class includes Matérn (Stein, 1999), Cauchy (Chiles and Delfiner, 2012), and Confluent Hypergeometric (Ma and Bhadra, 2023) covariance functions. We next consider an asymmetric version.

Proposition 2. Suppose that one can represent $C_{jk}^{\Re}(\mathbf{h}) = \int_0^\infty \exp(-v\|\mathbf{h}\|^2) g(v)du$ for $\mathbf{h} \in \mathbb{R}^d$ and $g(v)$ is a nonnegative density. Suppose also that the spectral density of $C_{jk}^{\Re}(\mathbf{h})$ exists. Then the corresponding asymmetric part based on the Fourier multiplier $-\text{isign}(\langle \mathbf{x}, \tilde{\mathbf{x}} \rangle)$ is $C_{jk}^{\Im}(\mathbf{h}) = \int_0^\infty \exp(-v\|\mathbf{h}\|^2) \text{erfi}(\sqrt{v}\langle \mathbf{h}, \tilde{\mathbf{x}} \rangle) g(v)dv$.

This gives three ways to find a $C_{jk}^{\Im}(\mathbf{h})$ in closed form: through the Fourier transform with multiplier $-\text{isign}(\langle \mathbf{x}, \tilde{\mathbf{x}} \rangle)$, through the scale-mixture representation $g(v)$ in Proposition 2, and through the Hilbert transform of $C_{jk}^{\Re}(\mathbf{h})$.

3.2 Cauchy covariance

We next apply Proposition 2 to the Cauchy covariance, defined as $C(\mathbf{h}) = \sigma (1 + a^2\|\mathbf{h}\|^2)^{-\alpha}$ for $\alpha > 0$ and $a > 0$. This covariance has been useful to model heavier tail decay (Lim and Teo, 2009; Chiles and Delfiner, 2012).

Proposition 3. The function $C_{jk}^{\Re}(h) = (1 + a^2\|\mathbf{h}\|^2)^{-\alpha}$ has an asymmetric part corresponding to

the Fourier multiplier $-\text{isign}(\langle \mathbf{x}, \tilde{\mathbf{x}} \rangle)$ of

$$C_{jk}^{\mathfrak{R}}(\mathbf{h}) = \frac{1}{(a^2\|\mathbf{h}\|^2 + 1)^\alpha} \frac{2}{\sqrt{\pi}} \frac{\Gamma(\alpha + \frac{1}{2})}{\Gamma(\alpha)} \frac{a\langle \mathbf{h}, \tilde{\mathbf{x}} \rangle}{(a^2\|\mathbf{h}\|^2 + 1)^{\frac{1}{2}}} {}_2F_1\left(\frac{1}{2}, \frac{1}{2} + \alpha; \frac{3}{2}; \frac{a^2\langle \mathbf{h}, \tilde{\mathbf{x}} \rangle^2}{a^2\|\mathbf{h}\|^2 + 1}\right),$$

where ${}_2F_1(a, b; c; z)$ is the hypergeometric function (Abramowitz and Stegun, 1948).

This form consists of $C_{jk}^{\mathfrak{R}}(\mathbf{h})$ multiplied by a relatively complicated expression. We next consider a few special cases with simpler forms.

Example 1 (Special case $d = 1$). When $d = 1$, from 15.8.1 of DLMF we have:

$$C_{jk}^{\mathfrak{R}}(\mathbf{h}) = \frac{2}{\sqrt{\pi}} \frac{\Gamma(\alpha + \frac{1}{2})}{\Gamma(\alpha)} a h {}_2F_1\left(\alpha + \frac{1}{2}, 1; \frac{3}{2}; -a^2 h^2\right),$$

which corresponds to the Hilbert transform (2.56) of King (2009).

Example 2 (Special case $\alpha = 1$). Consider the case $\alpha = 1$ where $C_{jk}^{\mathfrak{R}}(\mathbf{h}) = (a^2\|\mathbf{h}\|^2 + 1)^{-1}$. Applying 15.1.8 of Abramowitz and Stegun (1948) results in

$$C_{jk}^{\mathfrak{R}}(\mathbf{h}) = \frac{1}{a^2\|\mathbf{h}\|^2 + 1} \frac{a\langle \mathbf{h}, \tilde{\mathbf{x}} \rangle}{\sqrt{a^2(\|\mathbf{h}\|^2 - \langle \mathbf{h}, \tilde{\mathbf{x}} \rangle^2) + 1}}.$$

When $d = 1$, this matches with the one-dimensional Hilbert transform as entry (2.4) in the tables of King (2009).

Example 3 (Special case $\alpha = 1/2$). Consider the case $\alpha = 1/2$ where $C_{jk}^{\mathfrak{R}}(\mathbf{h}) = (a^2\|\mathbf{h}\|^2 + 1)^{-1/2}$. Then, 15.1.4 and 4.6.22 of Abramowitz and Stegun (1948) imply

$$C_{jk}^{\mathfrak{R}}(\mathbf{h}) = \frac{1}{\sqrt{a^2\|\mathbf{h}\|^2 + 1}} \frac{2}{\pi} \tanh^{-1}\left(\frac{a\langle \mathbf{h}, \tilde{\mathbf{x}} \rangle}{\sqrt{a^2\|\mathbf{h}\|^2 + 1}}\right).$$

In the case that $d = 1$, one has $C_{jk}^{\mathfrak{R}}(\mathbf{h}) = (a^2h^2 + 1)^{-1/2}(2/\pi) \sinh^{-1}(ah)$, again matching a one-dimensional Hilbert transform entry (2.54) in King (2009).

The Examples 2 and 3 for $d = 2$ are plotted in Figure 1. In these cases, evaluation of the asymmetric part does not involve any special functions.

3.3 Matérn covariance

The Matérn covariance, defined as $C_{jk}^{\mathfrak{R}}(\mathbf{h}) = 2^{1-\nu} \Gamma(\nu)^{-1} (a\|\mathbf{h}\|)^\nu K_\nu(a\|\mathbf{h}\|)$, is a key model used in spatial statistics and related fields (Porcu et al., 2024), where $K_\nu(z)$ is the modified Bessel function of the second kind. Asymmetric forms were studied and plotted carefully in Yarger et al. (2026). We present these results. While closed form $C_{jk}^{\mathfrak{R}}(\mathbf{h})$ remain limited to $d = 1$, $C_{jk}^{\mathfrak{R}}(\mathbf{h})$ can be computed efficiently for $d = 2$ through fast Fourier transforms (Yarger et al., 2026), which we use for Figure 1.

Example 4 (Matérn). Suppose that $\nu \notin \{1/2, 3/2, \dots\}$ and $d = 1$. Then, based on (8I.2) of King (2009) and 3.771.1 of Gradshteyn and Ryzhik (2014) we have

$$C_{jk}^{\mathfrak{S}}(h) = \frac{\pi \operatorname{sign}(h)}{2^\nu \Gamma(\nu) \cos(\pi\nu)} (a|h|)^\nu \{I_\nu(a|h|) - L_{-\nu}(a|h|)\},$$

where $I_\nu(z)$ is a modified Bessel and $L_\nu(z)$ is a modified Struve function (DLMF).

The gives the asymmetric Matérn cross-covariance for most $\nu > 0$. We next present $\nu = 1/2$, where the Matérn covariance reduces to an exponential covariance.

Example 5 (Exponential). Take $\nu = 1/2$ and $d = 1$ with $C_{jk}^{\mathfrak{R}}(h) = \exp(-a|h|)$. Then we have

$$C_{jk}^{\mathfrak{S}}(h) = \frac{\operatorname{sign}(h)}{\pi} \{\exp(a|h|)E_1(a|h|) + \exp(-a|h|)\operatorname{Ei}(a|h|)\},$$

where $E_1(z)$ and $\operatorname{Ei}(z)$ are commonly-defined exponential integrals (Chapter 6 of DLMF). This follows from the Hilbert transform (3.3) in the tables of King (2009).

For $d > 1$, the desired form for the Matérn implied by Proposition 2 is

$$C_{jk}^{\mathfrak{S}}(\mathbf{h}) = \frac{1}{2^{2\nu} \Gamma(\nu)} \int_0^\infty \exp(-v\|\mathbf{h}\|^2) \operatorname{erfi}(\sqrt{v}\langle \mathbf{h}, \tilde{\mathbf{x}} \rangle) v^{\nu-1} \exp\left(-\frac{1}{4v}\right) dv.$$

The integral's value has been determined in the case where $\langle \mathbf{h}, \tilde{\mathbf{x}} \rangle = \|\mathbf{h}\|$ to match the $d = 1$ case (for example, 1.17.71 of Oberhettinger and Badii, 2012), but the extension to general $\langle \mathbf{h}, \tilde{\mathbf{x}} \rangle$ does not appear to be established.

3.4 Other covariance functions

In Yarger and Bhadra (2025), fast Fourier transforms were used to compute $C_{jk}^{\mathfrak{S}}(\mathbf{h})$ for the Confluent Hypergeometric covariance function, which has control over both the origin and tail behavior of the covariance. However, closed forms of $C_{jk}^{\mathfrak{S}}(\mathbf{h})$ were not established. While the mixing density $g(v)$ is Beta-prime (Theorem 1 of Ma and Bhadra, 2023), the integral corresponding to Proposition 2 is unclear.

Compact covariance functions, where $C_{jk}^{\mathfrak{R}}(\mathbf{h}) = 0$ for all $\|\mathbf{h}\| > c$ for some $c > 0$, have also been proposed in spatial or temporal settings (e.g. Bevilacqua et al., 2025; Faouzi et al., 2025). By introducing zero entries in the covariance matrix, matrix calculations can be improved with these covariance functions. A compactly supported $C_{jk}^{\mathfrak{R}}(\mathbf{h})$ does not usually translate to a compactly supported $C_{jk}^{\mathfrak{S}}(\mathbf{h})$. For example, consider the triangular function $C_{jk}^{\mathfrak{R}}(h) = (1 - |h|)\mathbb{I}(0 \leq |h| < 1)$, which is a valid covariance function for (only) $d = 1$ (Chiles and Delfiner, 2012). It has Hilbert transform (9.6) of King (2009):

$$C_{jk}^{\mathfrak{S}}(h) = \frac{1}{\pi} \left(\log \left| \frac{1+h}{1-h} \right| + h \log \left| \frac{h^2 - 1}{h^2} \right| \right),$$

which satisfies $C_{jk}^{\mathfrak{S}}(h) = 0$ only when $h = 0$.

3.5 Multivariate nonseparability and flexibility

Above, we assumed throughout that $f_j(\mathbf{x}) = f_k(\mathbf{x})$. In Appendix A.1, we present the results when the squared-exponential ($a_j \neq a_k$), Cauchy ($a_j \neq a_k$, $\alpha_j \neq \alpha_k$), and Matérn ($a_j \neq a_k$, $\nu_j \neq \nu_k$) covariances have different parameters. As presented above, we need only check if σ , corresponding to (3), is Hermitian and positive definite for validity. However, consider that $\tilde{\mathbf{x}}$ may vary across cross-covariances, denoted $\tilde{\mathbf{x}}_{jk} = \tilde{\mathbf{x}}_{kj}$ for $j \neq k$. In this case for $p \geq 3$, one needs the positive-definiteness for all relevant $\mathbf{x} \in \mathbb{R}^d$ of $[\Re(\sigma_{jk}) - \text{i}\text{sign}(\langle \mathbf{x}, \tilde{\mathbf{x}}_{jk} \rangle)\Im(\sigma_{jk})]_{j,k=1}^p$.

4 Reflective asymmetric univariate space-time covariances

We next discuss the univariate space-time setting; the asymmetric functions in the previous section will be our building blocks for asymmetry in space-time covariances. We will use a_s (a_t) as an inverse spatial (temporal) range parameter where necessary to distinguish, as well as marginal covariances $C_s(\mathbf{h})$ and $C_t(u)$.

We propose this construction for asymmetric models in the spectral domain:

$$f(\mathbf{x}, \eta) = \sigma f^*(\|\mathbf{x}\|, |\eta|) \{1 + \xi \text{sign}(\langle \mathbf{x}, \tilde{\mathbf{x}} \rangle) \text{sign}(\eta)\}, \quad (4)$$

where $f^*(\|\mathbf{x}\|, |\eta|)$ is the symmetric spectral density of a space-time covariance, $\sigma > 0$ is a variance parameter, $\xi \in (-1, 1)$ is an asymmetry parameter with $\xi = 0$ corresponding to symmetry, and $\tilde{\mathbf{x}}$ is again a fixed unit vector of length d . We demonstrate the applicability of Bochner's Theorem as presented in Theorem 2.

- (a) The density is symmetric with respect to both arguments at the same time: $f(-\mathbf{x}, -\eta) = \sigma f^*(\|-\mathbf{x}\|, |-\eta|) \{1 + \xi(-1)(-1) \text{sign}(\langle \mathbf{x}, \tilde{\mathbf{x}} \rangle) \text{sign}(\eta)\} = f(\mathbf{x}, \eta)$.
- (b) The positivity and integrability of $f(\mathbf{x}, \eta)$ is ensured when $f^*(\|\mathbf{x}\|, |\eta|)$ is positive and integrable. As $0 < 1 - |\xi| \leq 1 + \xi \text{sign}(\langle \mathbf{x}, \tilde{\mathbf{x}} \rangle) \text{sign}(\eta) \leq 1 + |\xi| < 2$ for $\xi \in (-1, 1)$, one has $(1 - |\xi|)\sigma f^*(\|\mathbf{x}\|, |\eta|) \leq f(\mathbf{x}, \eta) \leq (1 + |\xi|)\sigma f^*(\|\mathbf{x}\|, |\eta|)$.

We outline specific forms of these models, at first when $f^*(\|\mathbf{x}\|, |\eta|)$ is separable.

4.1 Separable-type models

We first consider building space-time models of the form (4) based on separable covariance models, where $f^*(\|\mathbf{x}\|, |\eta|) = f_s(\|\mathbf{x}\|)f_t(|\eta|)$, and the integrals separate:

$$\begin{aligned} C(\mathbf{h}, u) &= \sigma \int_{\mathbb{R}^d} \exp(\text{i}\langle \mathbf{h}, \mathbf{x} \rangle) f_s(\|\mathbf{x}\|) d\mathbf{x} \int_{\mathbb{R}} \exp(\text{i}u\eta) f_t(|\eta|) d\eta \\ &\quad + \sigma\xi \int_{\mathbb{R}^d} \exp(\text{i}\langle \mathbf{h}, \mathbf{x} \rangle) \text{sign}(\langle \mathbf{x}, \tilde{\mathbf{x}} \rangle) f_s(\|\mathbf{x}\|) d\mathbf{x} \int_{\mathbb{R}} \exp(\text{i}u\eta) \text{sign}(\eta) f_t(|\eta|) d\eta \end{aligned}$$

$$=: \sigma \left\{ C_s^{\Re}(\mathbf{h}) C_t^{\Re}(u) + \xi C_s^{\Im}(\mathbf{h}) C_t^{\Im}(u) \right\}. \quad (5)$$

This covariance is a sum of two separable parts, one symmetric and the other asymmetric, and is no longer separable when $\xi \neq 0$. In this form of (5), the key observation is that the spatial and temporal parts correspond to cross-covariances in Section 3, as $\text{sign}(\langle \mathbf{x}, \tilde{\mathbf{x}} \rangle) \text{sign}(\eta) = -\{-\text{isign}(\langle \mathbf{x}, \tilde{\mathbf{x}} \rangle)\} \{-\text{isign}(\eta)\}$. We present an example from the large variety of combinations of covariances that may be chosen.

Example 6. Suppose we take a squared-exponential spatial covariance and a Cauchy temporal covariance with $\alpha = 1/2$: $C_s^{\Re}(\mathbf{h}) = \exp(-a_s^2 \|\mathbf{h}\|^2)$ and $C_t^{\Re}(u) = (a_t^2 u^2 + 1)^{-1/2}$. The corresponding asymmetric separable-type space-time covariance is

$$C(\mathbf{h}, u) = \sigma \frac{\exp(-a_s^2 \|\mathbf{h}\|^2)}{\sqrt{a_t^2 u^2 + 1}} \left\{ 1 + \xi \text{erfi}(a_s \langle \mathbf{h}, \tilde{\mathbf{x}} \rangle) \frac{2}{\pi} \sinh^{-1}(a_t u) \right\}.$$

We next plot Example 6 with $d = 1$ as an illustrative example in Figure 2. Interestingly, the asymmetric part can introduce negative covariance for some spatial and temporal lags. Negative correlation in space-time covariances is considered previously in [Mateu et al. \(2008\)](#) and [Horrell and Stein \(2017\)](#), for example.

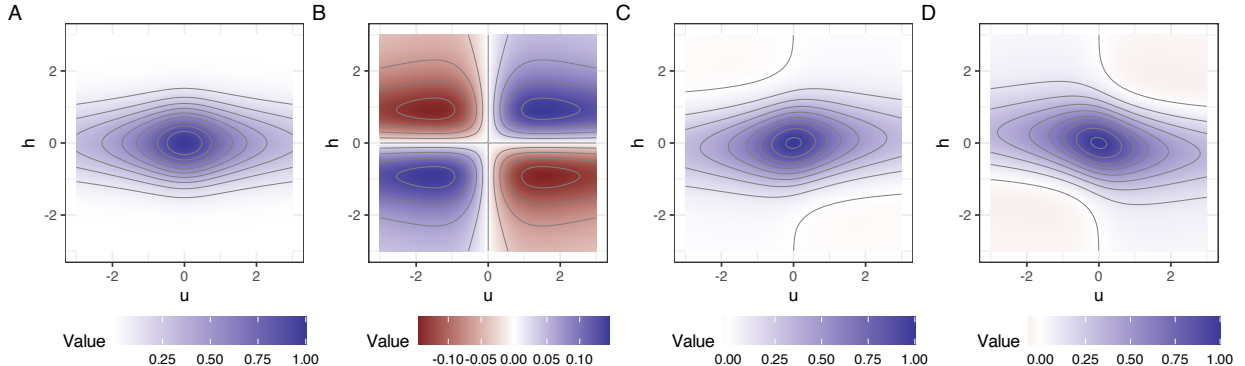


Figure 2: Separable-type covariances for $d = 1$ and plots based on squared-exponential (spatial) and Cauchy (temporal) model with $a_s = a_t = 1$, $\alpha = 1/2$, and $\sigma = 1$. (A) The symmetric case $\xi = 0$, (B) the asymmetric part only when taking $\xi = 1$ for illustration, (C) $\xi = 0.4$, (D) $\xi = -0.9$.

We discuss a few additional properties of the general model for any such separable-type construction.

Remark 1 (Separability). When we take (5), $C_s^{\Im}(\mathbf{0}) = C_t^{\Im}(0) = 0$, and $C_s^{\Re}(\mathbf{0}) = C_t^{\Re}(0) = 1$, the separability measure becomes $R(\mathbf{h}, u) = [\sigma]^2 \xi C_s^{\Im}(\mathbf{h}) C_t^{\Im}(u)$, and thus introduces both positive and negative separability (as in Figure 2).

Remark 2 (Axial symmetry). If $\xi \neq 0$, the covariance function is spatially axially symmetric (as in Definition 4 and [Park and Fuentes, 2008](#)) for the k -th dimension if and only if the k -th entry of $\tilde{\mathbf{x}}$ is 0.

Remark 3 (Marginal covariances). The marginal covariances are retained by the introduction of asymmetry: $C(\mathbf{h}, 0) = \sigma C_s^{\Re}(\mathbf{h})$ and $C(\mathbf{0}, u) = \sigma C_t^{\Re}(u)$, as $C_s^{\Im}(\mathbf{0}) = C_t^{\Im}(0) = 0$, assuming one has chosen $C_s^{\Re}(\mathbf{0}) = C_t^{\Re}(0) = 1$ without loss of generality.

We give another example in Figure 3 with $d = 2$. Asymmetry is introduced along the direction $\tilde{\mathbf{x}} = (1, 1)^\top / \sqrt{2}$, while the covariance is symmetric along $(1, -1)^\top / \sqrt{2}$.

These models represent a simple construction to introduce asymmetry in common separable space-time covariances. There are only $1 + (d - 1)$ additional parameters needed to describe the covariance through ξ (the asymmetry strength) and $\tilde{\mathbf{x}}$ (the asymmetry direction for $d > 1$), compared to the $O(d^2)$ parameters in the full Lagrangian model. The parameters $(\xi, \tilde{\mathbf{x}})$ represent the same model as $(-\xi, -\tilde{\mathbf{x}})$, so one may choose to reparameterise so that $0 \leq \xi < 1$ after estimation.

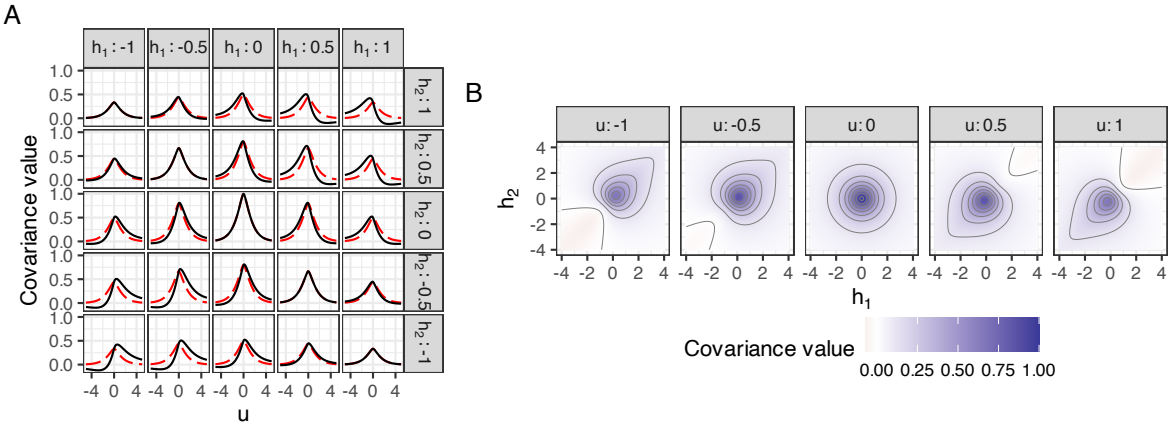


Figure 3: Cross-sections of the separable-type covariances for $d = 2$ using the Cauchy (spatial) and Matérn (temporal) model with $a_s = a_t = 1$, $\alpha = 1$, $\nu = 1$, $\sigma = 1$, $\tilde{\mathbf{x}} = (1, 1)^\top / \sqrt{2}$ and $\xi = -0.9$. (A) Covariance as a function of u for varying $\mathbf{h} = (h_1, h_2)^\top$, with the symmetric model $\xi = 0$ also plotted in dashed red; (B) covariance as a function of \mathbf{h} for varying u .

4.2 Squared-exponential and Cauchy asymmetric Gneiting models

We establish more involved asymmetric covariances of the Gneiting covariance type (Gneiting, 2002). Now $\sigma f^*(\|\mathbf{x}\|, |\eta|)$ represents the spectral density of a form of (1). Here, the integrals across \mathbf{x} and η will not separate resulting in a more challenging form. The closed forms are limited to $d = 1$, but we provide some half-spectral densities for general d in Appendix A.3. We focus on the choice of $\gamma(u) = a_t^2 u^2$, whose form is among recent Gneiting models studied (Allard et al., 2025).

Proposition 4 ($d = 1$ squared-exponential). Consider the Gneiting model in (1) with $d = 1$ and $\varphi(a_s \|\mathbf{h}\|^2) = \exp(-a_s^2 \|\mathbf{h}\|^2)$. The asymmetric squared-exponential covariance where $\gamma(u) = a_t^2 u^2$ is:

$$C(\mathbf{h}, u) = \sigma \frac{1}{\sqrt{a_t^2 u^2 + 1}} \exp\left(-\frac{a_s^2 h^2}{a_t^2 u^2 + 1}\right) \left\{ 1 + \xi \operatorname{erf}\left(\frac{a_s h}{\sqrt{a_t^2 u^2 + 1}} a_t u\right) \right\}.$$

This form now involves the regular error function which is also odd for $y \in \mathbb{R}$: $\text{erf}(y) = -\text{erf}(-y)$. The asymmetric part of the covariance is also nonseparable. Since $|\text{erf}(y)| \leq 1$ for all $y \in \mathbb{R}$, the covariance satisfies $C(h, u) \geq 0$ for all h and u , in contrast to Example 6. As suggested in Gneiting (2002), one can consider a version with a separability parameter $b \in [0, 1]$, with $b = 0$ corresponding to separability.

Example 7 ($d = 1$ squared-exponential, separability parameter). Let $b \in [0, 1]$, $\delta > 0$, and $\tau = b/2 + \delta > b/2$. Then we have the valid space-time covariance

$$C(h, u) = \frac{\sigma}{(a_t^2 u^2 + 1)^\tau} \exp \left\{ -\frac{a_s^2 h^2}{(a_t^2 u^2 + 1)^b} \right\} \left[1 + \xi \text{erf} \left\{ \frac{a_s h}{(a_t^2 u^2 + 1)^{\frac{b}{2}}} a_t u \right\} \right].$$

We plot examples of this model in Figure 4, where $\xi = b = 0$ corresponds to separability, and $\xi = 0$ corresponds to symmetry. The model gives intricate control of both the nonseparability and asymmetry.

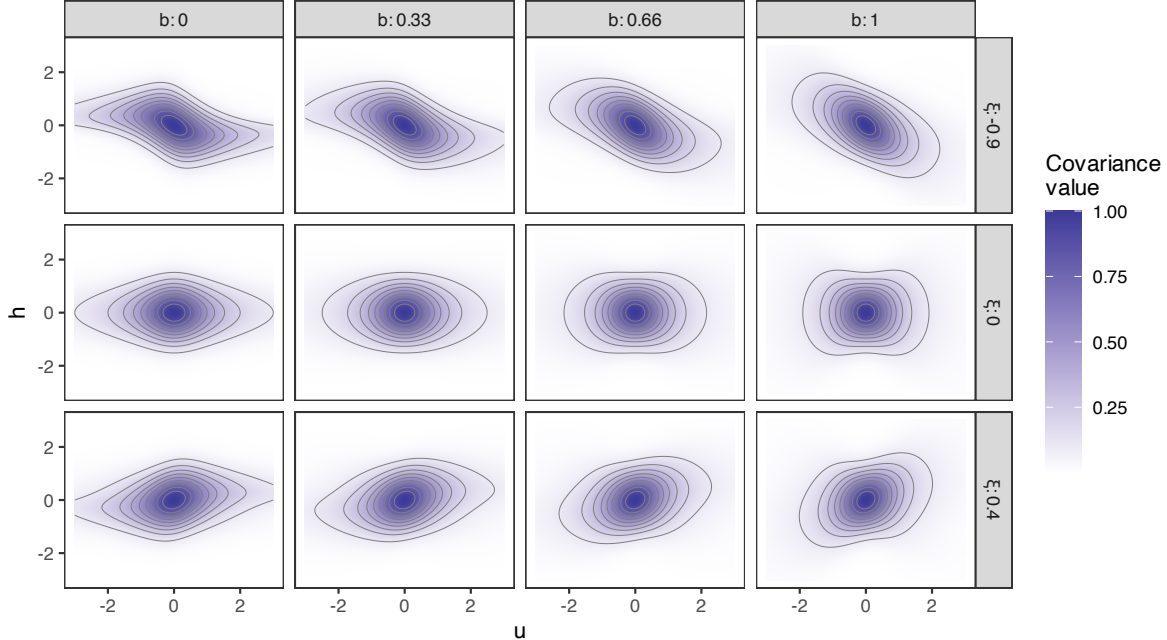


Figure 4: Gneiting-type covariances as in Example 7 with separability parameter b and asymmetry parameter ξ for $d = 1$ with $a_s = a_t = 1$, $\sigma = 1$, and $\delta = 1$.

We present a Cauchy covariance by mixing the form of Proposition 4. Additional versions, including for general α , are given in Appendix A.2.

Example 8 ($\alpha = 1/2$, $d = 1$ Cauchy). Let $h_* = h / \sqrt{a_t^2 u^2 + 1}$. The Cauchy-Gneiting nonseparable covariance with $\alpha = 1/2$ is

$$C(h, u) = \frac{\sigma}{\sqrt{a_t^2 u^2 + 1}} \frac{1}{\sqrt{a_s^2 h_*^2 + 1}} \left\{ 1 + \xi \frac{2}{\sqrt{\pi}} \frac{\sqrt{a_s^2 h_*^2 + 1}}{a_t u a_s h_*} \sinh^{-1} \left(\frac{a_t^2 u^2 a_s^2 h_*^2}{a_s^2 h_*^2 + 1} \right) \right\}$$

if $h \neq 0$ and $u \neq 0$. If $h = 0$ or $u = 0$, we have $C(h, u) = \sigma / \left(\sqrt{a_t^2 u^2 + 1} \sqrt{a_s^2 h_*^2 + 1} \right)$.

These forms extend a few Gneiting covariances with only one additional parameter ξ . Explicit forms for $d > 1$ require further study.

5 Practical considerations

We next discuss three practical aspects of the new space-time models: unconditional simulation, nonstationary and anisotropic models, and computational details.

5.1 Efficient spectral simulation

We propose the following algorithm for simulating random fields with separable-type asymmetric covariance. For $\ell = 1, 2, \dots, L$, we simulate $\phi_\ell \sim \text{Uniform}[0, 2\pi]$, $\psi_\ell \sim \text{Uniform}[0, 2\pi]$, $\mathbf{x}_\ell \sim g_s$, and $\eta_\ell \sim g_t$, where all are independent from each other. Here g_s and g_t are spatial and temporal proposal densities, respectively. Following [Emery et al. \(2016\)](#) for the spatial case, we propose to simulate:

$$Y(\mathbf{s}, t) = \frac{\sigma}{\sqrt{L}} \sum_{\ell=1}^L 2 \cos(\langle \mathbf{s}, \mathbf{x}_\ell \rangle + \phi_\ell) \cos(t\eta_\ell + \psi_\ell) \sqrt{\frac{f_s(\|\mathbf{x}_\ell\|)}{g_s(\|\mathbf{x}_\ell\|)} \frac{f_t(|\eta_\ell|)}{g_t(|\eta_\ell|)}} \\ + \frac{\sigma\xi}{\sqrt{L}} \sum_{\ell=1}^L 2 \sin(\langle \mathbf{s}, \mathbf{x}_\ell \rangle + \phi_\ell) \sin(t\eta_\ell + \psi_\ell) \sqrt{\frac{f_s(\|\mathbf{x}_\ell\|)}{g_s(\|\mathbf{x}_\ell\|)} \frac{f_t(|\eta_\ell|)}{g_t(|\eta_\ell|)}} \text{sign}(\langle \mathbf{x}_\ell, \tilde{\mathbf{x}} \rangle) \text{sign}(\eta_\ell).$$

For each ℓ , arguments from [Emery et al. \(2016\)](#), including trigonometric identities, show the desired parts of the covariance can be represented in expectation. See also [Arroyo and Emery \(2021\)](#); [Emery and Arroyo \(2018\)](#); [Allard et al. \(2025\)](#), and extensions to Gneiting-type models as in [Allard et al. \(2020\)](#) may also be formulated. We give an example in Figure 5. With $\tilde{\mathbf{x}} = (1, 0)^\top$ and $\xi > 0$, there is more correlation between positive h_1 and positive u than negative h_1 and positive u , inducing, for example, a general left-to-right asymmetric movement over time.

5.2 Nonstationary and anisotropic models

For the spatial portion of the model, nonstationarity through geometric anisotropy may be introduced, where the covariance depends on the spatial locations in addition to the spatial lag \mathbf{h} (nonstationarity) and will satisfy $C(\mathbf{h}_1, 0) \neq C(\mathbf{h}_2, 0)$ for two $\mathbf{h}_1, \mathbf{h}_2 \in \mathbb{R}^d$ such that $\|\mathbf{h}_1\| = \|\mathbf{h}_2\|$ (anisotropy). See [Paciorek and Schervish \(2006\)](#), [Emery and Arroyo \(2018\)](#), and [Allard et al. \(2025\)](#), for example. In particular, one may specify a $d \times d$ spatially-varying positive-definite matrix Σ_s representing a particular Mahalanobis distance used at \mathbf{s} .

We start with the squared-exponential model by replacing the spectral density $f_s(\|\mathbf{x}\|)$ with $f_{s_1, s_2}(\mathbf{x}) = (2\sqrt{\pi})^{-d} |\Sigma_{s_1}|^{1/4} |\Sigma_{s_2}|^{1/4} \exp(-\mathbf{x}^\top \Sigma_{s_1, s_2} \mathbf{x}/4)$, where $\Sigma_{s_1, s_2} = (\Sigma_{s_1} + \Sigma_{s_2})/2$. It

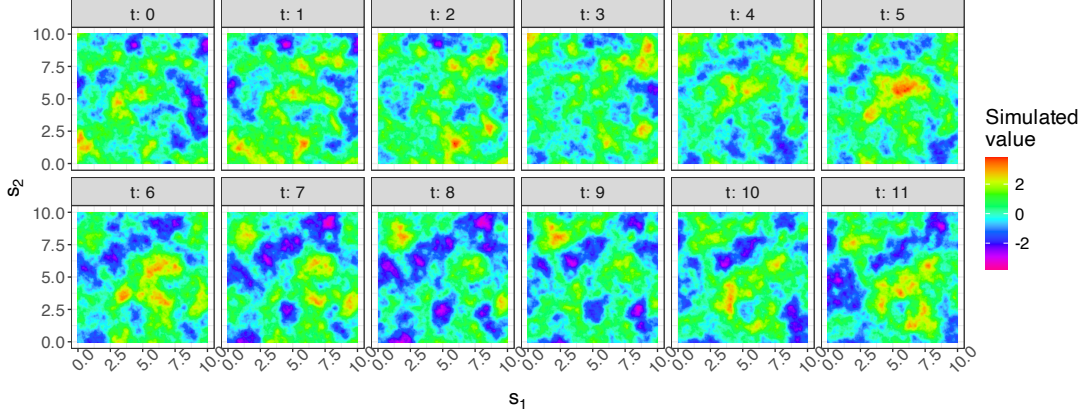


Figure 5: Simulation at different $(\mathbf{s} \in \mathbb{R}^2, t)$ on a grid of $301 \times 301 \times 12$. The spatial covariance is Matérn with $\nu_{\mathbf{s}} = 1$ and $a_{\mathbf{s}} = 1$. The temporal covariance is Matérn with $\nu_t = 2$ and $a_t = 1$. The other parameters are $\sigma = 1$, $\xi = 0.9$, $\tilde{\mathbf{x}} = (1, 0)^\top$. The proposals were Matérn spectral densities with $\nu = 0.5$ and $a = 1$, and $L = 30,000$.

straightforwardly follows from previous results in this paper that this gives an asymmetric covariance between locations \mathbf{s}_1 and \mathbf{s}_2 of $C_{\mathbf{s}_1, \mathbf{s}_2}(\mathbf{h}, u) = |\Sigma_{\mathbf{s}_1}|^{1/4} |\Sigma_{\mathbf{s}_2}|^{1/4} |\Sigma_{\mathbf{s}_1, \mathbf{s}_2}|^{-1/2} C(\Sigma_{\mathbf{s}_1, \mathbf{s}_2}^{-1/2} \mathbf{h}, u)$, where $C(\mathbf{h}, u)$ is a separable-type model from Section 4.1 with squared-exponential spatial covariance. The spatial asymmetric portion $C_{\mathbf{s}_1, \mathbf{s}_2}^{\mathfrak{S}}(\mathbf{h})$ is now reflected across the plane perpendicular to $\Sigma_{\mathbf{s}_1, \mathbf{s}_2}^{-1/2} \tilde{\mathbf{x}}$ instead of perpendicular to $\tilde{\mathbf{x}}$, inducing a spatially-varying asymmetry direction. In this formulation, the parameter $a_{\mathbf{s}}$ is absorbed into $\Sigma_{\mathbf{s}}$, and forms may be constructed for other classes (Emery and Arroyo, 2018). In Figure 6, we plot stationary ($\Sigma_{\mathbf{s}} = \Sigma$) asymmetric covariances with anisotropy.

5.3 Computational implementation

We discuss three computational aspects of the model. While the Lagrangian model (2) requires matrix operations of size $d \times d$ for each combination of u and \mathbf{h} , the evaluation of $C(\mathbf{h}, u)$ we introduce only requires the possible evaluation of special functions. We note that many functions involved in the asymmetric covariances are available in C++ (Johnson, 2025; Galassi et al., 2002) with interfaces in R (Eddelbuettel and Francois, 2023). In Table 1, we compare evaluation times in R using versions of $\text{erfi}(z)$ through Auguié et al. (2022) and Johnson (2025), the hypergeometric function through Hankin (2006), and the exponential integrals through Goulet (2016). For the special cases of the Cauchy model $\alpha = 1/2$ and $\alpha = 1$, evaluation of the asymmetric part takes essentially the same time as the symmetric part. Evaluation of the functions $\text{erfi}(z)$ (squared-exponential), ${}_2F_1(a, b; c, z)$ (Cauchy), and $\text{Ei}(z)$ and $E_1(z)$ (exponential) require additional computation time, especially for the hypergeometric function.

There is also a contrast with the Lagrangian model in terms of the number of covariance evaluations. In the setting where data is observed on a grid of space (of size n_s) and time (regularly-spaced of size n_t) with $n = n_s n_t$ total data points, the Lagrangian model requires computing (2)

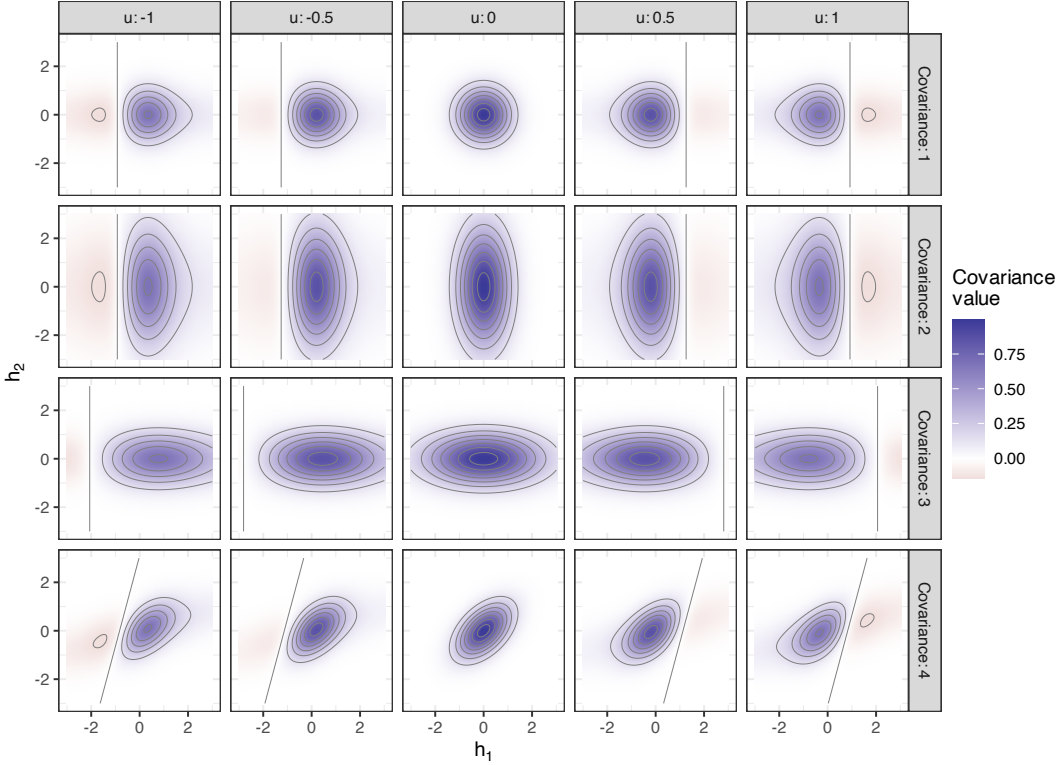


Figure 6: Space-time covariances with anisotropy. The spatial covariance is squared-exponential and the temporal is Matérn with parameter $\nu = 1$ and $a_t = 1$, with $\sigma = 1$, $\xi = -0.9$, and $\tilde{\mathbf{x}} = (1, 0)^\top$. The covariances 1 through 4 have $\Sigma = \text{diag}(1, 1)$, $\Sigma = \text{diag}(1, 5)$, $\Sigma = \text{diag}(5, 1)$, $\Sigma = [\mathbb{I}(i = j) + 0.5\mathbb{I}(i \neq j)]_{i,j=1}^2$, respectively.

Covariance Function	Function(s)	Implementation	$C_{jk}^{\Re}(h)$	$C_{jk}^{\Im}(h)$
Sq. Exp.	$\text{erfi}(z)$	(Rcpp)Faddeeva	0.069	0.152
Cauchy (α)	${}_2F_1(a, b; c; z)$	gsl	0.071	1.211
Cauchy ($\alpha = 1/2$)	$\sinh^{-1}(z)$	base	0.070	0.077
Cauchy ($\alpha = 1$)	z (linear)	base	0.064	0.066
Exponential	$\text{Ei}(z)$, $E_1(z)$	expint	0.065	0.157

Table 1: In seconds, the time of 50,000 evaluations of the cross-covariances components in $d = 1$.

on the order of $n_t n_s^2$ times to construct the covariance matrix of the data. For a separable-type model introduced here, the $n \times n$ symmetric covariance matrix may instead be represented using the Kronecker product \otimes : $\sigma \Psi_s^{\Re} \otimes \Psi_t^{\Re} + \sigma \xi \Psi_s^{\Im} \otimes \Psi_t^{\Im}$, where the matrices Ψ are $n_s \times n_s$ for the subscript s , $n_t \times n_t$ for the subscript t , symmetric for the superscript \Re , and skew-symmetric for the superscript \Im (the Kronecker product of two skew-symmetric matrices is symmetric). The order of the number of covariance evaluations is then $n_t + n_s^2$, a substantial reduction when n_t and n_s are both moderately large.

However, unlike the separable model, where the likelihood evaluation can be reduced to operations on matrices of size $n_s \times n_s$ and $n_t \times n_t$, when $\xi \neq 0$ the likelihood still requires decomposing

the full $n \times n$ matrix. This can be prohibitive when the total number of data points n is large. We propose to use Vecchia's approximation to make approximate likelihood inference manageable in this setting (Vecchia, 1988; Katsfuss et al., 2020). For this approximation, conditional independence is assumed between many data points based on a neighborhood structure. Vecchia's approximation for basic space-time models are implemented in, for example, the `GpGp` package in R (Guinness et al., 2021), as well as for Lagrangian models in Ma (2025). Idir et al. (2025) recently evaluate the choice of neighborhood structure for (symmetric) space-time models. We implement many of the newly introduced models within the framework of `GpGp` in C++, which enables large-scale data analysis later. The Kronecker product matrix representation does not necessarily apply within Vecchia's approximation, as an observation's neighbors generally will not be gridded.

6 Simulation studies

We next consider simulation studies for both multivariate spatial data and univariate space-time data. We discuss parameter estimation, improved model fit when there is asymmetry, and in the space-time setting that the new asymmetric models are substantially different from the Lagrangian space-time model.

6.1 Multivariate spatial simulation

We simulate bivariate spatial data according to the squared-exponential, Cauchy, and Matérn models with $d = 2$. For each, we consider $\Re(\sigma_{12}) \in \{-0.4, 0, 0.4\}$, $\Im(\sigma_{12}) \in \{0, 0.4\}$, $\sigma_{11} = \sigma_{22} = 1$, and $\tilde{\mathbf{x}} = (1, 1)^\top / \sqrt{2}$. A nugget variance of 0.1 is included for each process. We vary the sample size $n \in \{100, 200, 400, 600\}$, and take the two processes to be colocated with random uniform locations on $[0, 1] \times [0, 1]$. We take $a_1 = 12$ and $a_2 = 18$, using the cross-covariance forms in Appendix A.1, as well as $\alpha_1 = \alpha_2 = 1$ for the Cauchy and $\nu_1 = \nu_2 = 1$ for the Matérn. Simulations were replicated 100 times for each n , covariance, and configuration of σ_{12} .

We estimate asymmetric and symmetric versions of each model by maximum likelihood through the L-BFGS-B algorithm (Byrd et al., 1995). For the Matérn model, a fast Fourier transform is used to compute the covariance on a regular grid, which is then interpolated onto the lags in the data. In the optimization, the asymmetry direction is estimated as $\tilde{\mathbf{x}} = \{\sin(\zeta), \cos(\zeta)\}^\top$ through the single parameter ζ . We evaluate estimation of the asymmetric cross-covariance in Figure 7. In general, the asymmetric model has much better fit in terms of the Akaike information criterion (AIC) when the sample size is large enough and there is an asymmetric portion to the model. When there is no asymmetric portion, the AIC is slightly worse due to the increased number of parameters. Furthermore, for each of the covariance classes, the parameter $|\Im(\sigma_{12})|$ appears to be estimable, with improved estimation as n increases. In Appendix B.1, we also plot AIC when the covariance class is misspecified and evaluate a likelihood ratio test for asymmetry.

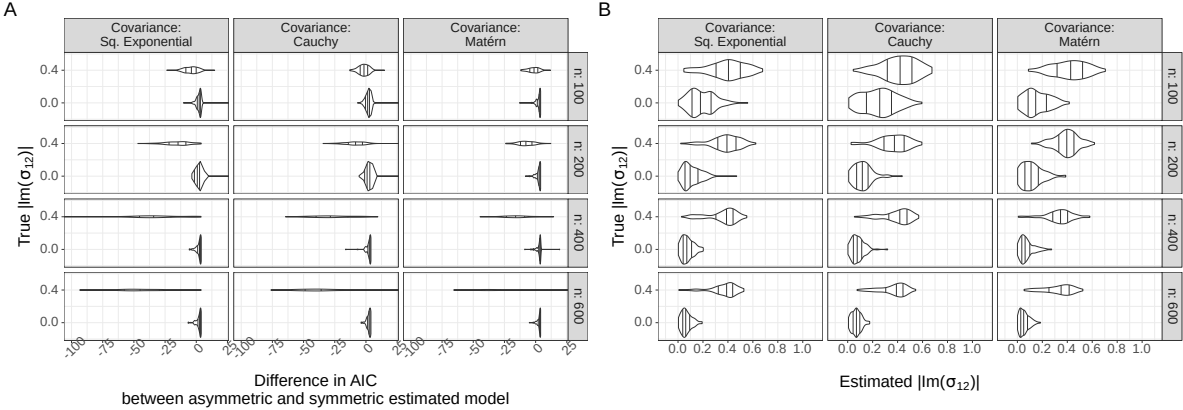


Figure 7: Multivariate spatial simulation results. Lines on violin plots represent the 0.25, 0.50, and 0.75 quantiles. (A) AIC comparison of asymmetric and symmetric models when the covariance class is correctly specified and $\Re(\sigma_{12}) = 0.4$. (B) Estimates of $|\Im(\sigma_{12})|$ when the covariance class is correctly specified and $\Re(\sigma_{12}) = 0.4$. Note $\Im(\sigma_{12})$ might only be identified up to a sign.

6.2 Univariate space-time simulation

We next consider a space-time model with spatial dimension $d = 1$. We take consider sample sizes of size $n = n_s n_t$, with $n_s \in \{20, 50, 100\}$ and $n_t = 25$. Locations in space and time are generated on $[0, 1]$. We consider when the observations are colocated (a two-dimensional random grid of dimensions n_s and n_t is used) or not colocated ($n_s n_t$ observations generated uniformly and independently on $[0, 1] \times [0, 1]$).

We simulate response data $Y(s, t)$ for 100 replications according to symmetric and asymmetric versions of the squared-exponential, Cauchy, exponential, and Gneiting squared-exponential (as in Example 7) covariances. We take $\sigma = 1$ and $\xi \in \{0, 0.4, 0.8\}$. We take $a_s = 10$ and $a_t = 15$. For the Gneiting model, we take $\tau = 1/2$ and $b = 0.7$. In addition, we simulate according to a squared-exponential Lagrangian model (2) with $\mathbb{E}(V) = 5$ and $\text{Var}(V) = 225$. This choice of $\text{Var}(V) = 225$ approximately matches the choice of $a_t = 15$ considering the correspondence between Lagrangian and Gneiting covariances when $\mathbb{E}(V) = 0$ (Salvà and Genton, 2021).

We consider estimation of symmetric and asymmetric versions of the models using the direct covariances without Vecchia's approximation, with results presented in Figure 8. Similar to the multivariate spatial case, the symmetric and asymmetric versions perform similarly in terms of AIC when the true model is symmetric. However, when there is asymmetry, estimating the asymmetric part can considerably improve model fit for each covariance class. We also provide a comparison with the Lagrangian covariance. When the covariance is symmetric and separable ($\xi = 0$), the Lagrangian model performs substantially worse than symmetric model in terms of AIC. This contrasts with the reflective asymmetric model, which has the separable, symmetric model is nested inside of it. When the true covariance is Lagrangian, the symmetric and reflective asymmetric covariance models perform somewhat worse than the Lagrangian model. These results suggest that, while incorporating asymmetry into space-time covariances is important, the type of asymmetry

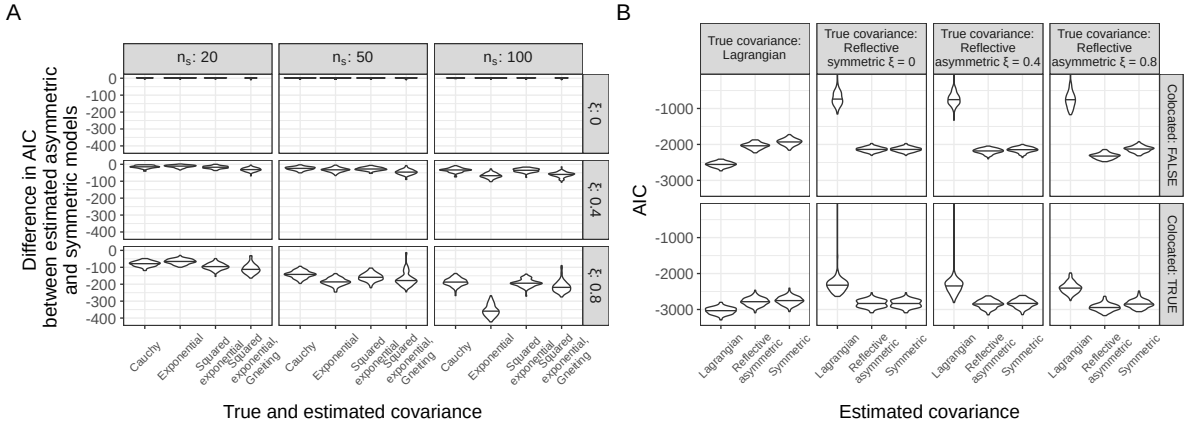


Figure 8: Univariate space-time simulation results. The lines represent medians. (A) AIC comparison of the asymmetric and symmetric models when the covariance class is correctly specified and observations are not colocated. (B) AIC comparison of the Lagrangian and reflective asymmetric squared-exponential models when $n_s = 100$.

specified can also play a outsized role in model fit. In Appendix B.1, we evaluate the likelihood ratio test for asymmetry based on the symmetric and reflective asymmetric models. In general, we find that the test performs well when the covariance class is correctly specified in terms of Type I error rate and power, though Type I error may be somewhat inflated if there is misspecification of the covariance function class.

7 Data analysis

The Irish wind data, originally studied in [Haslett and Raftery \(1989\)](#), has frequently been used as a dataset for evaluation in the space-time covariance literature ([Gneiting, 2002](#); [Gneiting et al., 2006](#); [Ma, 2025](#)). The data consist of 11 locations with daily wind data from 1961 to 1978. We follow similar pre-processing as [Gneiting et al. \(2006\)](#). The years 1961–1970 are used as training data, and to create mean-zero residuals, we subtract off a location effect and 6 seasonal harmonics after applying a square root transformation. Locations ($d = 2$) were translated from longitude and latitude to distance in kilometers in the cardinal directions.

We aim to estimate the model by maximum likelihood using the L-BFGS-B algorithm ([Byrd et al., 1995](#)). However, the dataset consists of $n_t = 3,652$ time points at the $n_s = 11$ locations, with $n = n_s n_t = 40,172$ not amenable to full likelihood inference. We thus use the Vecchia implementation mentioned in Section 5.3, with 30 neighbors primarily chosen using the temporal dimension. That is, most of (s_i, t_j) 's neighbors consist of $\{(s_{i*}, t_j), (s_{i*}, t_j - 1), (s_{i*}, t_j + 1)\}$, for different s_{i*} . The covariances are listed in Table 2. This includes various reflective separable-type asymmetric models and their separable, symmetric counterparts. We include models in GpGp of `exponential_spacetime` and `matern_spacetime`, which take $C(\mathbf{h}, u) = \sigma C_0 \left(\sqrt{a_s^2 \|\mathbf{h}\|^2 + a_t^2 u^2} \right)$, where $C_0(z)$ is an exponential or Matérn covariance. We also implement the Lagrangian model (2).

For all models, we use the same neighbors and include a location-specific and time-specific nugget effect with variance τ^2 .

Cov (\mathbf{h})	Cov (u)	Type	$\ell(\hat{\boldsymbol{\theta}} \mathbf{Y})$	Parameters	AIC	Time (secs)
Sq. Exp.	Cauchy ($\alpha_t = 1$)	Sym	-18256	4	36520	8
Sq. Exp.	Cauchy ($\alpha_t = 1$)	Asym	-18092	6	36196	40
Sq. Exp.	Cauchy ($\alpha_t = \frac{1}{2}$)	Sym	-18147	4	36302	9
Sq. Exp.	Cauchy ($\alpha_t = \frac{1}{2}$)	Asym	-17984	6	35979	60
Sq. Exp.	Sq. Exp.	Sym	-18565	4	37138	11
Sq. Exp.	Sq. Exp.	Asym	-18417	6	36845	60
Cauchy ($\alpha_s = \frac{1}{2}$)	Cauchy ($\alpha_t = \frac{1}{2}$)	Sym	-17375	4	34758	7
Cauchy ($\alpha_s = \frac{1}{2}$)	Cauchy ($\alpha_t = \frac{1}{2}$)	Asym	-17231	6	34475	42
Cauchy (α_s)	Cauchy (α_t)	Sym	-16430	6	32873	81
Cauchy (α_s)	Cauchy (α_t)	Asym	-16337	8	32690	2405
GpGp exponential_spacetime		Sym	-19323	4	38654	20
GpGp matern_spacetime		Sym	-18434	5	36878	1555
Lagrangian Sq. Exp.		Asym	-18269	8	36555	127

Table 2: Optimization summaries of the estimated covariance models, with the symmetric and corresponding reflective asymmetric models presented in the first ten rows. Cauchy models had the parameter α either fixed or estimated. The value $\ell(\hat{\boldsymbol{\theta}}|\mathbf{Y})$ is the maximised log-likelihood. The time unit is seconds.

We compare model summaries in Table 2. With the same number or fewer parameters, reflective asymmetric models with a Cauchy temporal covariance have higher log-likelihood than the Lagrangian model. Each reflective asymmetric model improves over its symmetric counterpart. The models which have both Cauchy spatial and temporal covariances outperform all other models in terms of AIC. In addition, many of the covariances provide improvement over the standard GpGp models. While the asymmetric models take more time, the difference is not drastic, with exception of the Cauchy model where α_s and α_t are estimated. All other reflective asymmetric models are estimated more quickly than the Lagrangian model.

Some selected covariance functions are compared in Figure 9. In general, the estimated marginal spatial covariance functions appear similar between symmetric and asymmetric versions of the model. All asymmetric models indicate generally higher correlation for positive u and positive East-West distance, compared to positive u and negative East-West distance. This matches the expected West-to-East direction of atmospheric flow. The Lagrangian model has elliptical contours everywhere, which is not generally the case for the reflective asymmetric models.

We present the estimated parameters in Table 3. The symmetric and asymmetric versions of the models have comparable variance, inverse range, and nugget variance parameters. Furthermore, when the spatial covariance is of the same form, the inverse range parameters are similarly estimated regardless of the temporal covariance used. The parameter ξ is estimated to be similarly strong for each of the new asymmetric models. The estimated parameter $\tilde{\mathbf{x}}$ points East in general as expected, matching the plot of covariance functions. The Cauchy models with α_s and α_t estimated have these parameters less than 1/2, suggesting heavier tail decay than this special case.

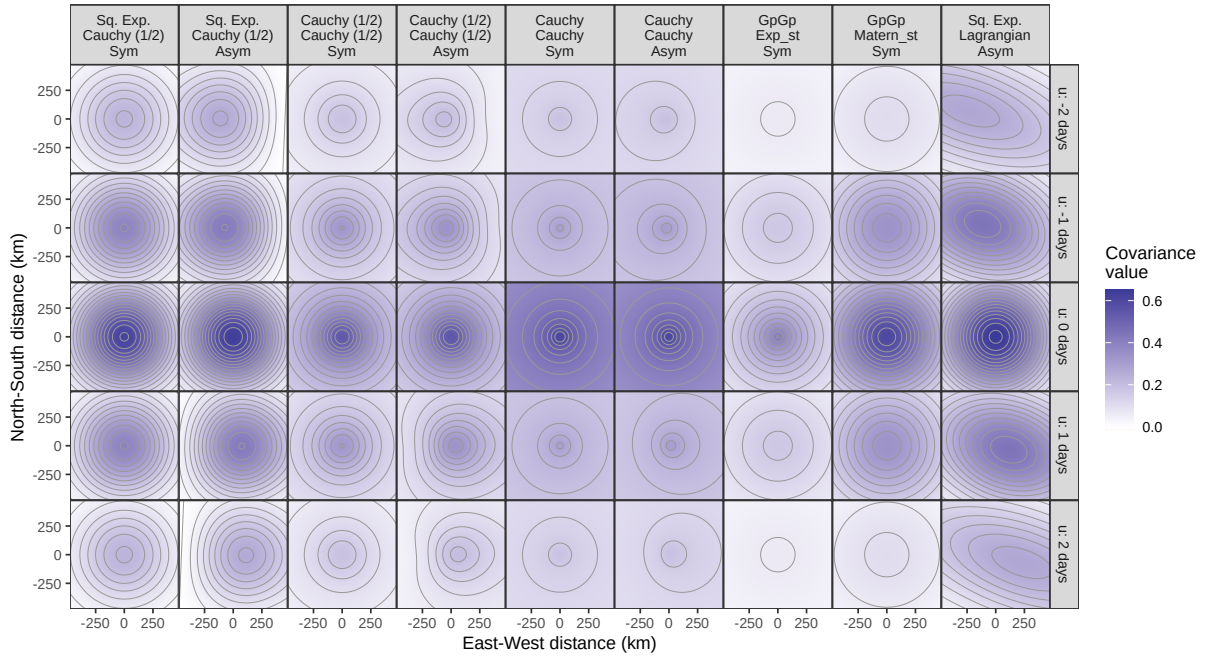


Figure 9: Selected estimated covariance functions $C(\mathbf{h}, u)$ plotted for different u for the Irish wind data. The top labels are the spatial covariance, temporal covariance, and if the covariance is symmetric or asymmetric, and match the order of Table 2.

In Appendix B.2, we present a prediction comparison, which shows improvements for asymmetric models.

8 Discussion

In this paper, we introduce a new approach that vastly increases the possible choices for asymmetric multivariate covariances and asymmetric space-time covariances. The key features of the new spatio-temporal models are flexibility over marginal covariance functions, model parsimony where asymmetric separable-type models represent a minimal increase of complexity over a separable model, and improvements in application and computation. Among other features, the model makes a likelihood ratio test for symmetry straightforward only involving the estimation of a symmetric and asymmetric model. Throughout, we make contrasts with the popular Lagrangian covariances that indicate a substantially different framework from them. We provide implementations both within and outside of the Vecchia approximation framework to make application to various space-time data feasible. In simulation studies and data analysis, we demonstrate that the models provide improved performance at times with faster computation. As in [Yarger et al. \(2026\)](#), a limitation is the lack of closed form Matérn asymmetric cross-covariances when $d > 1$. Addressing this, as well as establishing Gneiting-type asymmetric models for $d > 1$, would additionally expand applicability of these models.

A number of additional directions for methodological advancement are opened by this work. For

Cov (\mathbf{h})	Cov (u)	Type	σ	a_s	a_t	τ^2	ξ	atan2($\tilde{\mathbf{x}}$)
Sq. Exp.	Cauchy ($\alpha_t = 1$)	Sym	0.57	0.0024	0.84	0.07	-	-
Sq. Exp.	Cauchy ($\alpha_t = 1$)	Asym	0.59	0.0024	0.83	0.06	0.50	-1.6
Sq. Exp.	Cauchy ($\alpha_t = \frac{1}{2}$)	Sym	0.61	0.0024	1.23	0.07	-	-
Sq. Exp.	Cauchy ($\alpha_t = \frac{1}{2}$)	Asym	0.63	0.0024	1.20	0.06	0.50	-2.2
Sq. Exp.	Sq. Exp.	Sym	0.54	0.0024	0.84	0.06	-	-
Sq. Exp.	Sq. Exp.	Asym	0.55	0.0024	0.83	0.07	0.48	-3.3
Cauchy ($\alpha_s = \frac{1}{2}$)	Cauchy ($\alpha_t = \frac{1}{2}$)	Sym	0.54	0.0051	1.33	0.04	-	-
Cauchy ($\alpha_s = \frac{1}{2}$)	Cauchy ($\alpha_t = \frac{1}{2}$)	Asym	0.54	0.0051	1.31	0.04	0.46	3.0
Cauchy (α_s)	Cauchy (α_t)	Sym	0.61	0.0182	2.56	0.01	-	-
Cauchy (α_s)	Cauchy (α_t)	Asym	0.60	0.0170	2.38	0.02	0.42	8.1
GpGp exponential_spacetime		Sym	0.43	0.0025	0.93	0.00	-	-
GpGp matern_spacetime		Sym	0.60	0.0055	2.00	0.07	-	-
Lagrangian Sq. Exp.		Asym	0.65	0.0022	-	0.07	-	-

Table 3: Estimated covariance parameters. The column atan2($\tilde{\mathbf{x}}$) represents angle from the vector $(1, 0)^\top$ (directly East) converted to degrees. The symmetric and asymmetric Cauchy with general exponent had estimated $\alpha_s = 0.11$ and $\alpha_s = 0.11$, respectively, and $\alpha_t = 0.36$ and $\alpha_t = 0.37$, respectively. The additional parameters for the Lagrangian model were $\boldsymbol{\mu}_V = (114.0, -34.5)^\top$ in kilometers (corresponding to $\text{atan2}(\boldsymbol{\mu}_V) = -16.9$ degrees), and $(\boldsymbol{\Sigma}_V)_{11} = 111,921$, $(\boldsymbol{\Sigma}_V)_{22} = 12,701$, and $(\boldsymbol{\Sigma}_V)_{12} = (\boldsymbol{\Sigma}_V)_{21} = -37,666$. The GpGp matern_spacetime model had estimated parameter $\nu = 2.35$.

example, the extension to where the “temporal” dimension is Euclidean with dimension $\mathbf{u} \in \mathbb{R}^{d^*}$ and $d^* > 1$ is straightforward in this framework by using an appropriate choice of $\{C_t^{\Re}(\mathbf{u}), C_t^{\Im}(\mathbf{u})\}$. In addition, since the new models do not intersect with Lagrangian models, one could potentially combine these approaches for a very flexible asymmetric model. The extension to multivariate space-time models includes the possibility for developing additional types of asymmetries in space-time cross-covariance functions (Bourrotte et al., 2016).

Future research can evaluate these models in a large-scale data applications where handling nonstationarity and anisotropy is necessary and scientifically relevant. As the Irish wind data only included 11 locations, including nonstationary flexibility in space may not be sensible. However, an extensive data analysis of high-resolution climate model output (Donahue et al., 2024) or oceanographic data (Kuusela and Stein, 2018) could make full use of the nonstationary models.

References

M. Abramowitz and I. A. Stegun. *Handbook of Mathematical Functions with Formulas, Graphs, and Mathematical Tables*, volume 55. US Government printing office, 1948.

D. Allard, X. Emery, C. Lacaux, and C. Lantuéjoul. Simulating space-time random fields with nonseparable Gneiting-type covariance functions. *Statistics and Computing*, 30(5):1479–1495, Sept. 2020.

D. Allard, L. Clarotto, and X. Emery. Fully nonseparable Gneiting covariance functions for multivariate space-time data. *Spatial Statistics*, 52:100706, Dec. 2022. doi: 10.1016/j.spasta.2022.100706.

D. Allard, L. Benoit, and S. Obakrim. Modeling and simulating spatio-temporal, multivariate and nonstationary Gaussian Random Fields: A Gaussian mixtures perspective. *hal-05034982*, 2025.

T. V. Apanasovich, M. G. Genton, and Y. Sun. A valid Matérn class of cross-covariance functions for multivariate random fields with any number of components. *Journal of the American Statistical Association*, 107(497):180–193, 2012.

D. Arroyo and X. Emery. Algorithm 1013: An R implementation of a continuous spectral algorithm for simulating vector Gaussian random fields in Euclidean spaces. *ACM Transactions on Mathematical Software*, 47(1):1–25, Mar. 2021. doi: 10.1145/3421316.

B. Auguié, D. Eddelbuettel, and S. G. Johnson. *RcppFaddeeva*: ‘Rcpp’ Bindings for the ‘Faddeeva’ Package, 2022. URL <https://github.com/nano-optics/RcppFaddeeva>. R package version 0.2.3.

M. Bevilacqua, C. Caamaño-Carrillo, T. Faouzi, and X. Emery. Parsimonious compactly supported covariance models in the Gauss Hypergeometric Class: Identifiability, reparameterizations, and asymptotic properties. 2025. arXiv:2506.13646.

M. Bourotte, D. Allard, and E. Porcu. A flexible class of non-separable cross-covariance functions for multivariate space-time data. *Spatial Statistics*, 18:125–146, Nov. 2016. doi: 10.1016/j.spasta.2016.02.004.

R. H. Byrd, P. Lu, J. Nocedal, and C. Zhu. A limited memory algorithm for bound constrained optimization. *SIAM Journal on Scientific Computing*, 16(5):1190–1208, 1995.

W. Chen, M. G. Genton, and Y. Sun. Space-time covariance structures and models. *Annual Review of Statistics and Its Application*, 8:191–215, 2021.

J.-P. Chiles and P. Delfiner. *Geostatistics: Modeling Spatial Uncertainty*. John Wiley & Sons, 2012.

N. Cressie and H.-C. Huang. Classes of nonseparable, spatio-temporal stationary covariance functions. *Journal of the American Statistical Association*, 94(448):1330–1339, 1999.

S. De Iaco and D. Posa. Positive and negative non-separability for space-time covariance models. *Journal of Statistical Planning and Inference*, 143(2):378–391, Feb. 2013. doi: 10.1016/j.jspi.2012.07.006.

DLMF. *NIST Digital Library of Mathematical Functions*. <http://dlmf.nist.gov/>, Release 1.1.3 of 2021-09-15, 2021. URL <http://dlmf.nist.gov/>. F. W. J. Olver, A. B. Olde Daalhuis, D. W. Lozier, B. I. Schneider, R. F. Boisvert, C. W. Clark, B. R. Miller, B. V. Saunders, H. S. Cohl, and M. A. McClain, eds.

A. S. Donahue, P. M. Caldwell, L. Bertagna, H. Beydoun, P. A. Bogenschutz, A. Bradley, T. C. Clevenger, J. Foucar, C. Golaz, O. Guba, et al. To exascale and beyond—The Simple Cloud-Resolving E3SM Atmosphere Model (SCREAM), a performance portable global atmosphere model for cloud-resolving scales. *Journal of Advances in Modeling Earth Systems*, 16(7):e2024MS004314, 2024.

D. Eddelbuettel and R. Francois. *RcppGSL: ‘Rcpp’ integration for ‘GNU GSL’ vectors and matrices*, 2023. URL <https://CRAN.R-project.org/package=RcppGSL>. R package version 0.3.13.

X. Emery and D. Arroyo. On a continuous spectral algorithm for simulating non-stationary Gaussian random fields. *Stochastic Environmental Research and Risk Assessment*, 32:905–919, 2018.

X. Emery, D. Arroyo, and E. Porcu. An improved spectral turning-bands algorithm for simulating stationary vector Gaussian random fields. *Stochastic Environmental Research and Risk Assessment*, 30:1863–1873, 2016.

X. Emery, E. Porcu, and P. White. New validity conditions for the multivariate Matérn coregionalization model, with an application to exploration geochemistry. *Mathematical Geosciences*, 54(6):1043–1068, 2022.

A. A. Ezzat, M. Jun, and Y. Ding. Spatio-temporal asymmetry of local wind fields and its impact on short-term wind forecasting. *IEEE Transactions on Sustainable Energy*, 9(3):1437–1447, 2018.

T. Faouzi, E. Porcu, and M. Bevilacqua. Space-time smoothness and parsimony in covariance functions. *Mathematical Methods in the Applied Sciences*, June 2025. doi: 10.1002/mma.11100.

M. Felsberg and G. Sommer. The monogenic signal. *IEEE Transactions on Signal Processing*, 49(12):3136–3144, 2002.

T. C. Fonseca and M. F. Steel. A general class of nonseparable space-time covariance models. *Environmetrics*, 22(2):224–242, 2011.

M. Galassi, J. Davies, J. Theiler, B. Gough, G. Jungman, P. Alken, M. Booth, F. Rossi, and R. Ulerich. *GNU Scientific Library Reference Manual (3rd Ed.)*. 2002.

J. García-Cuerva. *Weighted Norm Inequalities and Related Topics*, volume 116. Elsevier, 1985.

M. G. Genton and W. Kleiber. Cross-covariance functions for multivariate geostatistics. *Statistical Science*, 30(2):147–163, 2015. doi: 10.1214/14-STS487.

T. Gneiting. Nonseparable, stationary covariance functions for space-time data. *Journal of the American Statistical Association*, 97(458):590–600, June 2002. doi: 10.1198/016214502760047113.

T. Gneiting and A. E. Raftery. Strictly proper scoring rules, prediction, and estimation. *Journal of the American Statistical Association*, 102(477):359–378, Mar. 2007. doi: 10.1198/016214506000001437.

T. Gneiting, M. Genton, and P. Guttorp. Geostatistical space-time models, stationarity, separability, and full symmetry. In B. Finkenstädt, L. Held, and V. Isham, editors, *Statistical Methods for Spatio-Temporal Systems*, volume 107, pages 151–175. Chapman and Hall/CRC, Oct. 2006. doi: 10.1201/9781420011050.ch4.

T. Gneiting, W. Kleiber, and M. Schlather. Matérn cross-covariance functions for multivariate random fields. *Journal of the American Statistical Association*, 105(491):1167–1177, 2010.

V. Goulet. *expint: Exponential Integral and Incomplete Gamma Function*, 2016. URL <https://cran.r-project.org/package=expint>. R package version 0.1-8.

I. S. Gradshteyn and I. M. Ryzhik. *Table of Integrals, Series, and Products*. Academic Press, 2014.

G. H. Granlund and H. Knutsson. *Signal Processing for Computer Vision*. Springer Science & Business Media, 2013.

J. Guinness, M. Katzfuss, and Y. Fahmy. *GpGp: Fast Gaussian process computation using Vecchia's approximation*. 2021. R package version 0.4.0.

R. K. S. Hankin. Special functions in R: Introducing the gsl package. *R News*, 6:24–26, October 2006.

J. Haslett and A. E. Raftery. Space-time modelling with long-memory dependence: Assessing Ireland's wind power resource. *Journal of the Royal Statistical Society: Series C (Applied Statistics)*, 38(1):1–21, 1989.

M. T. Horrell and M. L. Stein. Half-spectral space-time covariance models. *Spatial Statistics*, 19: 90–100, 2017.

Y. M. Idir, O. Orfila, P. Chatellier, and V. Judalet. Improving spatio-temporal Gaussian Process modeling with Vecchia approximation: A low-cost sensor-driven approach to urban environmental monitoring. Nov. 2025. doi: 10.48550/arXiv.2511.22500.

S. G. Johnson. *Faddeeva Package*. 2025. C++, http://ab-initio.mit.edu/wiki/index.php/Faddeeva_Package.

M. Katzfuss, J. Guinness, W. Gong, and D. Zilber. Vecchia approximations of Gaussian-Process predictions. *Journal of Agricultural, Biological and Environmental Statistics*, 25(3):383–414, Sept. 2020.

F. W. King. *Hilbert Transforms*. Cambridge University Press, 2009.

N. E. Korotkov and A. N. Korotkov. *Integrals Related to the Error Function*. Chapman and Hall/CRC, 2020.

M. Kuusela and M. L. Stein. Locally stationary spatio-temporal interpolation of Argo profiling float data. *Proceedings of the Royal Society A: Mathematical, Physical and Engineering Sciences*, 474 (2220), Dec. 2018.

B. Li and H. Zhang. An approach to modeling asymmetric multivariate spatial covariance structures. *Journal of Multivariate Analysis*, 102(10):1445–1453, 2011. doi: <https://doi.org/10.1016/j.jmva.2011.05.010>.

S. Lim and L. Teo. Gaussian fields and Gaussian sheets with generalized Cauchy covariance structure. *Stochastic Processes and their Applications*, 119(4):1325–1356, Apr. 2009. doi: 10.1016/j.spa.2008.06.011.

P. Ma. Asymmetric space-time covariance functions via hierarchical mixtures. 2025. arXiv:2511.07959.

P. Ma and A. Bhadra. Beyond Matérn: On a class of interpretable Confluent Hypergeometric covariance functions. *Journal of the American Statistical Association*, 118(543):2045–2058, 2023.

J. Mateu, E. Porcu, and P. Gregori. Recent advances to model anisotropic space-time data. *Statistical Methods and Applications*, 17(2):209–223, May 2008. doi: 10.1007/s10260-007-0056-6.

W. Mu, J. Chen, E. S. Davis, K. Reed, D. Phanstiel, M. I. Love, and D. Li. Gaussian Processes for time series with lead-lag effects with applications to biology data. *Biometrics*, 81(1):ujae156, 2025.

F. Oberhettinger and L. Badii. *Tables of Laplace Transforms*. Springer Science & Business Media, 2012.

C. J. Paciorek and M. J. Schervish. Spatial modelling using a new class of nonstationary covariance functions. *Environmetrics*, 17(5):483–506, Aug. 2006. doi: 10.1002/env.785.

M. S. Park and M. Fuentes. Testing lack of symmetry in spatial-temporal processes. *Journal of Statistical Planning and Inference*, 138(10):2847–2866, 2008.

E. Porcu, R. Furrer, and D. Nychka. 30 years of space-time covariance functions. *Wiley Interdisciplinary Reviews: Computational Statistics*, 13(2):e1512, 2021.

E. Porcu, M. Bevilacqua, R. Schaback, and C. J. Oates. The Matérn model: A journey through statistics, numerical analysis and machine learning. *Statistical Science*, 39(3):469–492, 2024.

M. L. O. Salvaña and M. G. Genton. Lagrangian spatio-temporal nonstationary covariance functions. In A. Daouia and A. Ruiz-Gazen, editors, *Advances in Contemporary Statistics and Econometrics*. Springer, 2021.

M. L. O. Salvaña, A. Lenzi, and M. G. Genton. Spatio-temporal cross-covariance functions under the Lagrangian framework with multiple advections. *Journal of the American Statistical Association*, 118(544):2746–2761, 2023.

M. Schlather. Some covariance models based on normal scale mixtures. 2010.

M. L. Stein. *Interpolation of Spatial Data: Some Theory for Kriging*. Springer Science & Business Media, 1999.

M. L. Stein. Space-time covariance functions. *Journal of the American Statistical Association*, 100(469):310–321, 2005.

A. V. Vecchia. Estimation and model identification for continuous spatial processes. *Journal of the Royal Statistical Society Series B: Statistical Methodology*, 50(2):297–312, 1988.

Q. Vu, A. Zammit-Mangion, and N. Cressie. Modeling nonstationary and asymmetric multivariate spatial covariances via deformations. *Statistica Sinica*, 32(4):2071–2093, 2022. doi: 10.5705/ss.202020.0156.

Z. Wu. *Non-Fully Symmetric Space-Time Matern-Cauchy Correlation Functions*. PhD thesis, Purdue University Graduate School, 2021.

D. Yarger and A. Bhadra. Multivariate Confluent Hypergeometric covariance functions with simultaneous flexibility over smoothness and tail decay. *Mathematical Geosciences*, 57:977–1001, 2025.

D. Yarger, S. Stoev, and T. Hsing. Multivariate Matérn models — A spectral approach. *Statistical Science*, 41(1):69–98, 2026. doi: 10.1214/24-STS948.

T. Zhang and H. Zhang. Non-fully symmetric space-time Matérn covariance functions. 2017.

X. Zhang, M. L. O. Salvaña, A. Lenzi, and M. G. Genton. Corrections to “Spatio-temporal cross-covariance functions under the Lagrangian framework with multiple advections”. *Journal of the American Statistical Association*, 119(548):3189–3189, Oct. 2024. doi: 10.1080/01621459.2024.2412190.

A Additional information on models

A.1 Cross-covariances between covariances with different parameters

We present cross-covariance forms for when the spectral densities of the original densities are not proportional with $f_j(\mathbf{x}) \neq f_k(\mathbf{x})$. We begin with the squared-exponential. Suppose that

$C_{jj}(\mathbf{h}) = \exp(-a_j^2 \|\mathbf{h}\|^2)$ and $C_{kk}(\mathbf{h}) = \exp(-a_k^2 \|\mathbf{h}\|^2)$ for parameters a_j and a_k . Let $a_{jk} = a_j a_k / \sqrt{(a_j^2 + a_k^2)/2}$. Then the corresponding components of the cross-covariance are:

$$C_{jk}^{\Re}(\mathbf{h}) = \left\{ \frac{a_{jk}}{(a_j a_k)^{\frac{1}{2}}} \right\}^d \exp(-a_{jk}^2 \|\mathbf{h}\|^2);$$

$$C_{jk}^{\Im}(\mathbf{h}) = \left(\frac{a_{jk}}{(a_j a_k)^{\frac{1}{2}}} \right)^d \exp(-a_{jk}^2 \|\mathbf{h}\|^2) \operatorname{erfi}(a_{jk} \langle \mathbf{h}, \tilde{\mathbf{x}}_{jk} \rangle),$$

where $\tilde{\mathbf{x}}_{jk} = \tilde{\mathbf{x}}_{kj}$. In general, the expression $\Re(\sigma_{jk})(a_{jk}/\sqrt{a_j a_k})^d$ now corresponds to the marginal covariance $\operatorname{Cov}\{Y_j(\mathbf{s}), Y_k(\mathbf{s})\}$ between processes j and k .

Now, consider the Cauchy covariance, where

$$C_{jj}(\mathbf{h}) = (a_j^2 \|\mathbf{h}\|^2 + 1)^{-\alpha_j}; \quad C_{kk}(\mathbf{h}) = (a_k^2 \|\mathbf{h}\|^2 + 1)^{-\alpha_k}.$$

Suppose that a_{jk} is defined as above and $\alpha_{jk} = (\alpha_j + \alpha_k)/2$. Then valid cross-covariance components are defined by

$$C_{jk}^{\Re}(\mathbf{h}) = \frac{a_{jk}^{2\alpha_{jk}}}{a_j^{\alpha_j} a_k^{\alpha_k}} \frac{\Gamma(\alpha_{jk})}{\sqrt{\Gamma(\alpha_j)\Gamma(\alpha_k)}} \frac{1}{(a_{jk}^2 \|\mathbf{h}\|^2 + 1)^{\alpha_{jk}}},$$

and

$$C_{jk}^{\Im}(\mathbf{h}) = C_{jk}^{\Re}(\mathbf{h}) \frac{2}{\sqrt{\pi}} \frac{\Gamma(\alpha_{jk} + \frac{1}{2})}{\Gamma(\alpha_{jk})} \frac{a_{jk} \langle \mathbf{h}, \tilde{\mathbf{x}}_{jk} \rangle}{\left(a_{jk}^2 \|\mathbf{h}\|^2 + 1\right)^{\frac{1}{2}}} {}_2F_1\left(\frac{1}{2}, \frac{1}{2} + \alpha_{jk}; \frac{3}{2}; \frac{a_{jk}^2 \langle \mathbf{h}, \tilde{\mathbf{x}}_{jk} \rangle^2}{a_{jk}^2 \|\mathbf{h}\|^2 + 1}\right).$$

The form of $C_{jk}^{\Re}(\mathbf{h})$ matches the adjustment in Allard et al. (2025) up to reparameterization of the inverse range parameter.

For the Matérn covariance with $d = 1$, we have, with $\nu_{jk} = (\nu_j + \nu_k)/2$ and $a_{jk} = \sqrt{(a_j^2 + a_k^2)/2}$,

$$C_{jk}^{\Re}(h) = \frac{a_j^{\nu_j} a_k^{\nu_k}}{a_{jk}^{2\nu_{jk}}} \frac{\Gamma(\nu_{jk})}{\sqrt{\Gamma(\nu_j)\Gamma(\nu_k)}} \frac{2^{1-\nu_{jk}}}{\Gamma(\nu_{jk})} (a_{jk}|h|)^{\nu} K_{\nu}(a_{jk}|h|),$$

and, for $\nu_{jk} \notin \{1/2, 3/2, \dots\}$,

$$C_{jk}^{\Im}(h) = \frac{a_j^{\nu_j} a_k^{\nu_k}}{a_{jk}^{2\nu_{jk}}} \frac{\Gamma(\nu_{jk})}{\sqrt{\Gamma(\nu_j)\Gamma(\nu_k)}} \frac{\pi \operatorname{sign}(h)}{2^{\nu_{jk}} \Gamma(\nu_{jk}) \cos(\pi \nu_{jk})}$$

$$\times (a_{jk}|h|)^{\nu_{jk}} \{ I_{\nu_{jk}}(a_{jk}|h|) - L_{-\nu_{jk}}(a_{jk}|h|) \}.$$

For the exponential, $d = 1$, where $\nu_j = \nu_k = 1/2$ and $a_{jk} = \sqrt{(a_j^2 + a_k^2)/2}$, we have

$$C_{jk}^{\mathfrak{R}}(h) = \frac{\sqrt{a_j a_k}}{a_{jk}} \exp(-a_{jk}|h|),$$

and

$$C_{jk}^{\mathfrak{S}}(h) = \frac{\sqrt{a_j a_k}}{a_{jk}} \frac{\text{sign}(h)}{\pi} \{ \exp(a_{jk}|h|) E_1(a_{jk}|h|) + \exp(-a_{jk}|h|) \text{Ei}(a_{jk}|h|) \}.$$

A.2 Additional Gneiting-Cauchy models

We first present the Gneiting-Cauchy model for general α .

Proposition A1 ($d = 1$ Cauchy). In the setting with $d = 1$, the corresponding Cauchy space-time Gneiting covariance with $\gamma(u) = a_t^2 u^2$ can be written in terms of the hypergeometric function for general α :

$$C(h, u) = \frac{\sigma}{\sqrt{a_t^2 u^2 + 1}} \frac{1}{\left(\frac{a_s^2 h^2}{a_t^2 u^2 + 1} + 1\right)^\alpha} \left\{ 1 + \xi \text{sign}(h) \text{sign}(u) \frac{2}{\sqrt{\pi}} {}_2F_1\left(\frac{1}{2}, \alpha; \frac{3}{2}; -\frac{a_t^2 u^2 a_s^2 h^2}{a_s^2 h^2 + a_t^2 u^2 + 1}\right) \right\}.$$

Once again, simplified expressions for the special cases $\alpha = 1/2$ in the main text and $\alpha = 1$ below are derived straightforwardly from special cases of the hypergeometric function ${}_2F_1$ (Section 15.4, [DLMF](#)).

Example A1 ($\alpha = 1$, $d = 1$, Cauchy). The special case with $\alpha = 1$ is

$$C(h, u) = \frac{\sigma}{\sqrt{a_t^2 u^2 + 1}} \frac{1}{\left(\frac{a_s^2 h^2}{a_t^2 u^2 + 1} + 1\right)} \left\{ 1 + \xi \frac{2}{\sqrt{\pi}} \frac{\sqrt{a_s^2 h^2 + a_t^2 u^2 + 1}}{a_t u a_s h} \tan^{-1}\left(\frac{a_t^2 u^2 a_s^2 h^2}{a_s^2 h^2 + a_t^2 u^2 + 1}\right) \right\}.$$

Example A2 ($\alpha = 1/2$, $d = 1$ Cauchy with separability parameter). Let $b \in [0, 1]$, $\delta > 0$, and $\tau = b/2 + \delta > b/2$. Then we have the following valid space-time covariance, where now $h_* = h/(a_t^2 u^2 + 1)^{b/2}$:

$$C(h, u) = \frac{\sigma}{(a_t^2 u^2 + 1)^\tau} \frac{1}{\sqrt{a_s^2 h_*^2 + 1}} \left\{ 1 + \xi \frac{2}{\sqrt{\pi}} \frac{\sqrt{a_s^2 h_*^2 + 1}}{a_t u a_s h_*} \sinh^{-1}\left(\frac{a_t^2 u^2 a_s^2 h_*^2}{a_s^2 h_*^2 + 1}\right) \right\}$$

if $h_* \neq 0$ and $u \neq 0$. Otherwise, $C(h, u) = \sigma / \left\{ (a_t^2 u^2 + 1)^\tau \sqrt{a_s^2 h_*^2 + 1} \right\}$.

Similar forms may be constructed for other α .

A.3 Squared-exponential Gneiting half-spectral density

We present half-spectral ([Horrell and Stein, 2017](#)) densities, in which the time dimension of the spectral density is integrated out. This proposition is similar to Lemma 1 of [Allard et al. \(2020\)](#) for the Gneiting covariance and now includes an asymmetric part.

Proposition A2 (Half-spectral representation of Gneiting squared-exponential covariance). Consider the squared-exponential covariance for the spatial covariance $\varphi(a_s^2\|\mathbf{h}\|^2) = \exp(-a_s^2\|\mathbf{h}\|^2)$. For $\gamma(u) = a_t^2u^2$, the Gneiting space-time covariance with additional asymmetric part for the squared-exponential has representation

$$C(\mathbf{h}, u) = \sigma \int_{\mathbb{R}^d} \frac{\exp(\mathbf{i}\langle \mathbf{h}, \mathbf{x} \rangle)}{(2a_s\sqrt{\pi})^d} \exp\left\{-\frac{\|\mathbf{x}\|^2}{4a_s^2}(a_t^2u^2 + 1)\right\} \left\{1 + \xi \text{sign}(\langle \mathbf{x}, \tilde{\mathbf{x}} \rangle) \text{erfi}\left(\frac{\|\mathbf{x}\|}{2a_s}a_tu\right)\right\} d\mathbf{x}.$$

For $\gamma(u) = a_t|u|$, it instead has representation

$$C(\mathbf{h}, u) = \sigma \int_{\mathbb{R}^d} \frac{\exp(\mathbf{i}\langle \mathbf{h}, \mathbf{x} \rangle)}{(2a_s\sqrt{\pi})^d} \exp\left\{-\frac{\|\mathbf{x}\|^2}{4a_s^2}(a_t|u| + 1)\right\} \{1 + \xi \text{sign}(\langle \mathbf{x}, \tilde{\mathbf{x}} \rangle) Z(\mathbf{x}, u)\} d\mathbf{x},$$

$$Z(\mathbf{x}, u) = \frac{\text{sign}(u)}{\pi} \left\{ \exp\left(-\frac{\|\mathbf{x}\|^2}{4a_s^2}a_t|u|\right) \text{Ei}\left(\frac{\|\mathbf{x}\|^2}{4a_s^2}a_t|u|\right) - \exp\left(\frac{\|\mathbf{x}\|^2}{4a_s^2}a_t|u|\right) \text{Ei}\left(\frac{\|\mathbf{x}\|^2}{4a_s^2}a_t|u|\right) \right\},$$

where parts of $Z(\mathbf{x}, u)$ correspond to the asymmetric exponential cross-covariance.

In general, for any $\gamma(u) = (a_t|u|)^\beta$ for $0 < \beta \leq 2$, the new asymmetric portion of the half-spectral representation will be related to the Hilbert transform of the powered-exponential class $\exp\{-(a_t|u|)^\beta\}$, with the above corresponding to $\beta = 2$ and $\beta = 1$, respectively. The half-spectral representation makes computation of the covariance straightforward through fast Fourier transforms even if a closed-form representation is not available. Recently, constructions have often focused on this form of $\gamma(u) = (a_t|u|)^\beta$ (Allard et al., 2025).

A.4 Additional model plot

In Figure A1, we plot cross-sections of separable-type asymmetric covariance functions $C(h, u)$ in $d = 1$.

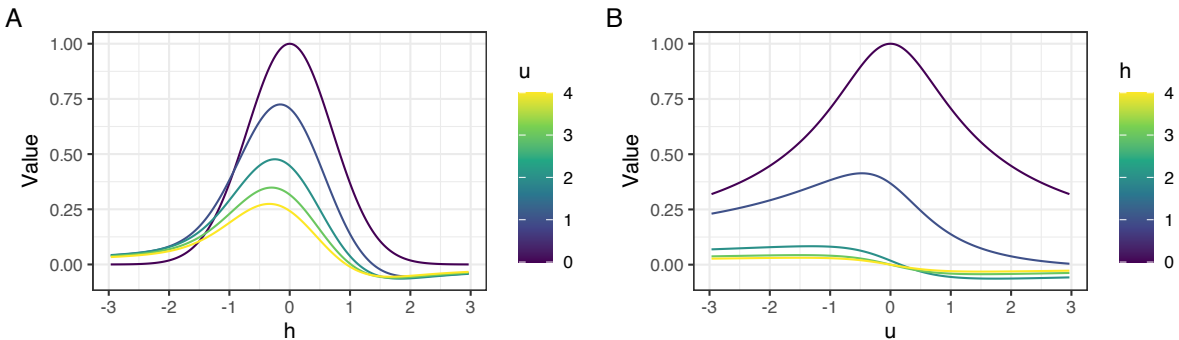


Figure A1: Cross-sections of the separable-type covariances for $d = 1$ using the squared-exponential (spatial) and Cauchy (temporal) model with $a_s = a_t = 1$, $\alpha = 1$, $\sigma = 1$, and $\xi = -0.9$. (A) Covariance as a function of h for varying u ; (B) covariance as a function of u for varying h .

B Additional empirical results

B.1 Additional simulation results

We plot AIC information for the multivariate spatial simulation including when the covariance function is misspecified in Figure B2. In general, including asymmetry in the model can still improve performance when the true model is asymmetric with a different covariance class. For example, the asymmetric Matérn provides performance near that of the squared-exponential when the true covariance is squared-exponential and $\Im(\sigma_{12}) = 0.4$. The Matérn and Cauchy perform similarly across most settings, while the squared-exponential has considerably higher AIC when the true covariance is Matérn.

In Tables B1, B2, and B3, we provide empirical size and power analyses for a likelihood ratio test in the multivariate and space-time simulation studies. In particular, we consider a chi-squared likelihood ratio test of level $\alpha = 0.05$. In general, we find that the test controls Type I error rate generally well when the covariance class is correctly specified, while it may be somewhat inflated if the covariance class is misspecified. Under the simulation settings, the test has more power in the space-time simulation, perhaps due to the larger total sample size $n = n_s \times n_t$.

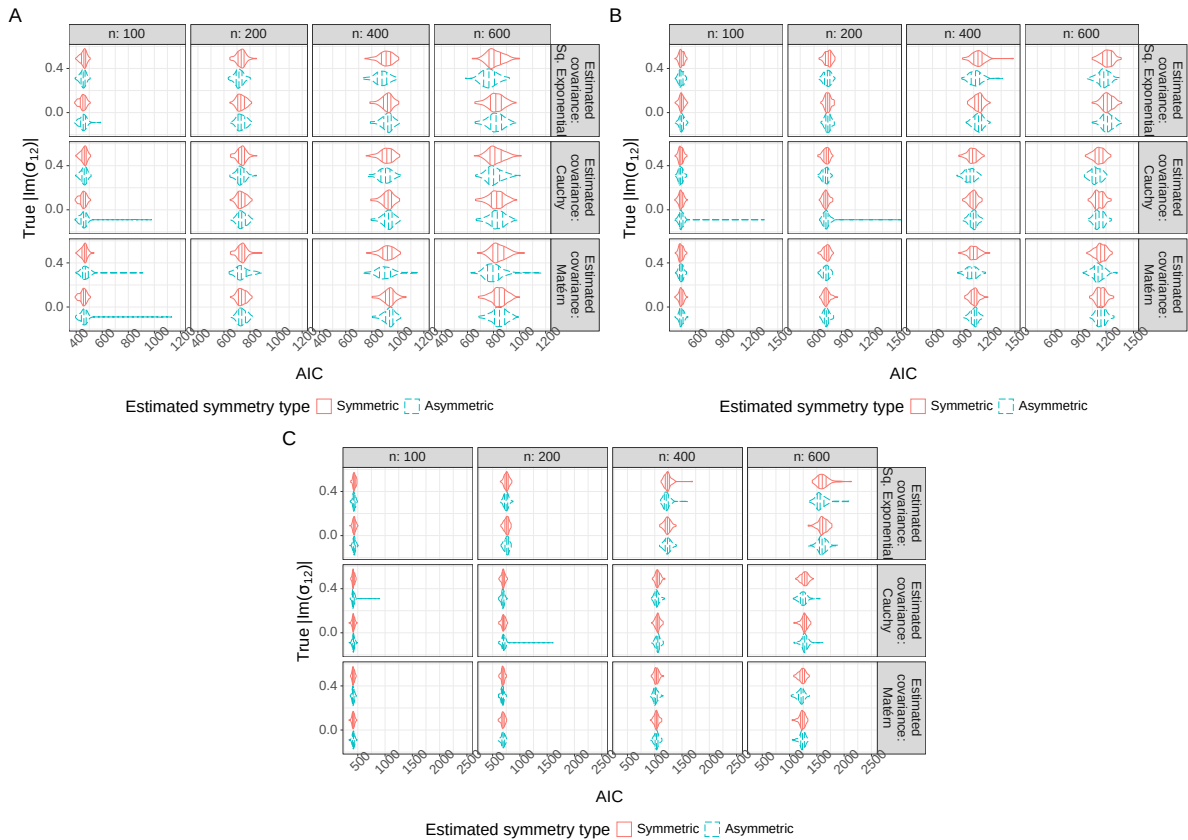


Figure B2: AIC for estimated multivariate spatial models when the true covariance is squared-exponential (A), Cauchy (B), and Matérn (C).

True covariance						
Class	Sq. Exp.		Cauchy		Matérn	
$\Im(\sigma_{12})$	0.00	0.40	0.00	0.40	0.00	0.40
LRT Sq. Exp.	0.06	0.90	0.04	0.83	0.10	0.80
LRT Cauchy	0.03	0.72	0.03	0.80	0.07	0.82
LRT Matérn	0.05	0.69	0.06	0.75	0.04	0.79

Table B1: For the multivariate spatial simulation study, the proportion of rejections for the chi-squared likelihood ratio tests at the 0.05 level when $n = 200$ and $\Re(\sigma_{jk}) = 0.4$. The likelihood ratio tests (LRTs) are based on the difference of log-likelihoods for the symmetric and reflective asymmetric multivariate covariances of the specified class.

True covariance									
Class	Sq. Exp.			Cauchy			Exponential		
ξ	0.00	0.40	0.80	0.00	0.40	0.80	0.00	0.40	0.80
LRT Sq. Exp.	0.05	0.98	1.00	0.12	0.98	1.00	0.06	0.76	1.00
LRT Cauchy	0.04	0.77	1.00	0.03	1.00	1.00	0.05	0.81	1.00
LRT Exponential	0.08	0.97	1.00	0.08	0.99	1.00	0.04	0.98	1.00
LRT Gneiting b	0.07	0.76	1.00	0.09	0.51	1.00	0.07	0.38	0.87
LRT Gneiting	0.09	0.84	1.00	0.37	0.74	0.97	0.27	0.46	0.89

Table B2: For the space-time simulation study, the proportion of rejections for the chi-squared likelihood ratio tests at the 0.05 level when $n_s = 20$ and locations are colocated. The likelihood ratio tests (LRTs) are based on the difference of log-likelihoods for the symmetric and reflective asymmetric covariances of the specified class, where Gneiting b refers to with the nonseparability parameter and Gneiting refers to without the nonseparability parameter.

B.2 Irish wind parameters and prediction study

We next present the prediction study. For a particular time t_{pred} , we use data from all $t < t_{pred}$ to predict $Y(\mathbf{s}, t)$ at times $Y(\mathbf{s}, t_{pred})$, $Y(\mathbf{s}, t_{pred} + 1)$, $Y(\mathbf{s}, t_{pred} + 2)$, \dots . We consider two settings. The first uses all locations $\{Y(\mathbf{s}, t)\}_{t < t_{pred}, \mathbf{s}}$ as prediction data for $Y(\mathbf{s}_{pred}, t_{pred})$. The second uses only data from other locations, using $\{Y(\mathbf{s}, t)\}_{t < t_{pred}, \mathbf{s} \neq \mathbf{s}_{pred}}$ for $Y(\mathbf{s}_{pred}, t_{pred})$. We refer to this as the leave-one-out setting, which is fundamentally more challenging than the first setting. We take t_{pred} to be each day from January 1st, 1971 to December 30th, 1978, where the mean function and covariance parameters were estimated from data before January 1st, 1971. This gives 2,922 total t_{pred} for each a prediction is formed for the subsequent days. Predictions for different t_{pred} may be computed in parallel.

To form predictions, we once again use Vecchia's approximation through [Guinness et al. \(2021\)](#). We use the same $m = 60$ neighbors for each method to compute conditional expectations of $Y(\mathbf{s}_{pred}, t_{pred})$. In addition, we use [Guinness et al. \(2021\)](#)'s conditional simulation with $m = 8$ to simulate 50 realizations from the conditional distribution of $Y(\mathbf{s}_{pred}, t_{pred})$, whose variance is used as a conditional variance. All distributions are taken to be Gaussian.

To evaluate the models, we use the continuous ranked probability score (CRPS) that takes into account the entire distributional prediction ([Gneiting and Raftery, 2007](#)), with smaller values

Class	Sq. Exp.	True covariance							
		Lagrangian		Gneiting b		Gneiting			
		ξ	-	0.00	0.40	0.80	0.00		
LRT Sq. Exp.			1.00	0.07	1.00	1.00	0.10	0.97	1.00
LRT Cauchy			1.00	0.10	1.00	1.00	0.11	0.97	1.00
LRT Exponential			0.99	0.15	0.98	1.00	0.12	0.96	1.00
LRT Gneiting b			1.00	0.12	1.00	1.00	0.04	1.00	0.99
LRT Gneiting			1.00	0.09	1.00	1.00	0.04	1.00	1.00

Table B3: For the space-time simulation study, the proportion of rejections for the chi-squared likelihood ratio tests at the 0.05 level when $n_s = 20$ and locations are colocated. The likelihood ratio tests (LRTs) are based on the difference of log-likelihoods for the symmetric and reflective asymmetric covariances of the specified class, where Gneiting b refers to with the nonseparability parameter and Gneiting refers to without the nonseparability parameter.

representing better prediction. We provide summaries of this score for the two settings, as well as for a different number of days in advance of prediction, plotted in Figure B3. In general, asymmetric versions of the model have improved prediction than their symmetric versions, especially when predicting just one day in advance. When all locations are used, the models with Cauchy spatial covariances perform the best. There are fewer differences in the leave-one-out setting, but the models with both squared-exponential spatial and temporal covariances lag behind other models. The asymmetric Lagrangian model performs well in the leave-one-out setting, but is worse than some reflective asymmetric models when using all locations for prediction. In general, prediction performance drops off quickly from one day in advance to two or three days in advance. As expected, the leave-one-out-setting has worse predictions than the all locations setting.

C Proofs

Proof of Proposition 1. We aim to compute

$$C_{jk}^{\mathfrak{S}}(\mathbf{h}) = \int_{\mathbb{R}^d} \exp(\mathfrak{i}\langle \mathbf{h}, \mathbf{x} \rangle) \{-\text{isign}(\langle \mathbf{x}, \tilde{\mathbf{x}} \rangle)\} \frac{1}{(2a\sqrt{\pi})^d} \exp\left(-\frac{\|\mathbf{x}\|^2}{4a^2}\right) d\mathbf{x}.$$

Consider the variable transformation $\mathbf{w} = (w_1, \dots, w_d)^\top = O\mathbf{x}$ where O is an orthonormal rotation matrix such that $\text{sign}(\langle \mathbf{x}, \tilde{\mathbf{x}} \rangle) = \text{sign}(\langle O^\top \mathbf{w}, \tilde{\mathbf{x}} \rangle) = \text{sign}(w_1)$. That is, we choose O such that the direction of w_1 aligns with $\tilde{\mathbf{x}}$. We have $\|\mathbf{x}\|^2 = \mathbf{x}^\top \mathbf{x} = \mathbf{w}^\top O O^\top \mathbf{w} = \mathbf{w}^\top \mathbf{w} = \|\mathbf{w}\|^2$, $\langle \mathbf{h}, O^\top \mathbf{w} \rangle = \mathbf{h}^\top O^\top \mathbf{w} = (O\mathbf{h})^\top \mathbf{w}$, and $d\mathbf{w} = |O| d\mathbf{x} = d\mathbf{x}$, so the integral is written

$$C_{jk}^{\mathfrak{S}}(\mathbf{h}) = \int_{\mathbb{R}^d} \exp(\mathfrak{i}\langle O\mathbf{h}, \mathbf{w} \rangle) \{-\text{isign}(w_1)\} \frac{1}{(2a\sqrt{\pi})^d} \exp\left(-\frac{\|\mathbf{w}\|^2}{4a^2}\right) d\mathbf{w}.$$

Now, break up the integral into $d - 1$ and 1 dimensions, letting the Hadamard product of \mathbf{w}

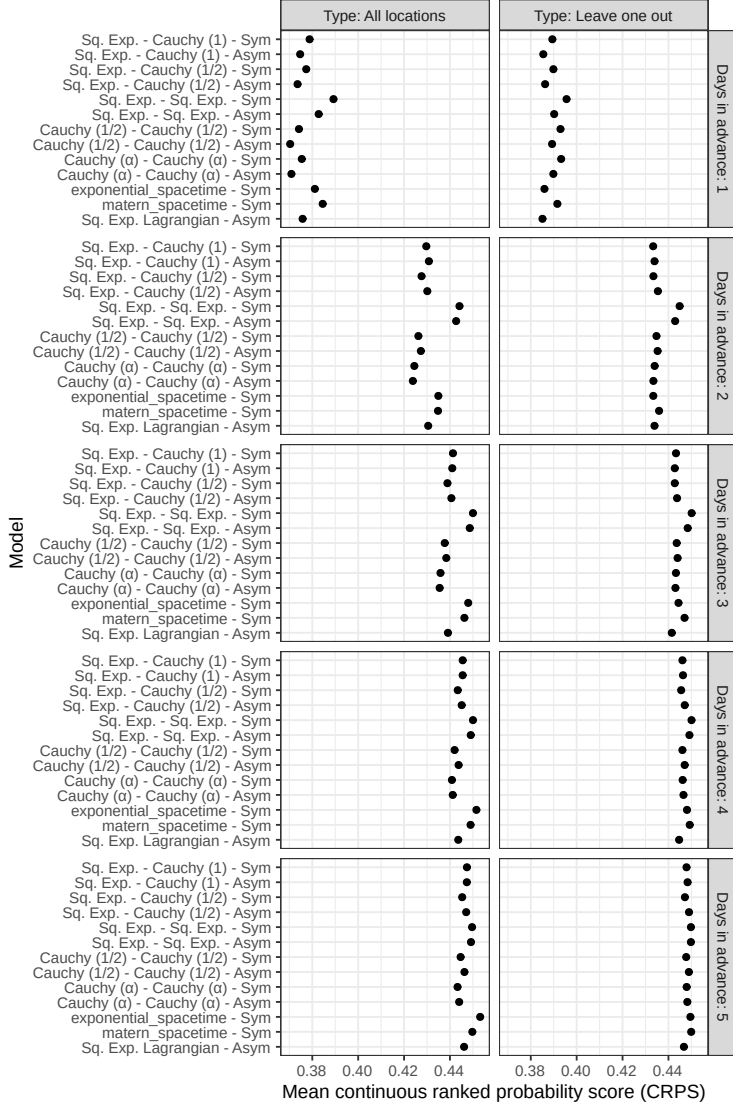


Figure B3: Prediction summaries for the Irish wind data across the study design and the number of days in advance the prediction was formed. The models are in the same order as Table 2

with the first standard basis vector be $\mathbf{w} \odot \mathbf{e}_1 = (w_1, 0, \dots, 0)^\top$:

$$C_{jk}^{\mathfrak{V}}(\mathbf{h}) = \left[\int_{\mathbb{R}} \exp(i\langle O\mathbf{h}, \mathbf{w} \odot \mathbf{e}_1 \rangle) \{-i\text{sign}(w_1)\} \frac{1}{2a\sqrt{\pi}} \exp\left(-\frac{w_1^2}{4a^2}\right) dw_1 \right] \\ \times \left[\int_{\mathbb{R}^{d-1}} \exp\{\mathfrak{i}\langle O\mathbf{h}, \mathbf{w} - \mathbf{w} \odot \mathbf{e}_1 \rangle\} \frac{1}{(2a\sqrt{\pi})^{d-1}} \exp\left(-\frac{\sum_{j=2}^d w_j^2}{4a^2}\right) dw_2 \dots dw_d \right].$$

The second integral (which is separated as it does not technically depend on w_1) just corresponds with the Gaussian spectral density in $d-1$ dimensions with the first entry of $O\mathbf{h}$ zeroed out, resulting in $\exp(-a^2\|O\mathbf{h} - [O\mathbf{h} \odot \mathbf{e}_1]\|^2)$. The first integral corresponds to the $d=1$ asymmetric case applied to the first entry $O\mathbf{h} \odot \mathbf{e}_1$: $\exp(-a^2\|O\mathbf{h} \odot \mathbf{e}_1\|^2) \text{erfi}(a [\mathbf{h}^\top O^\top \mathbf{e}_1])$. As $O\mathbf{h} \odot \mathbf{e}_1$ and $O\mathbf{h} - O\mathbf{h} \odot$

e_1 are orthogonal, the product of the two integrals is $C_{jk}^{\mathfrak{I}}(\mathbf{h}) = \exp(-a^2\|\mathbf{O}\mathbf{h}\|^2) \operatorname{erfi}(a\mathbf{h}^\top \mathbf{O}^\top e_1)$. Converting back into the original orientation we have $C_{jk}^{\mathfrak{I}}(\mathbf{h}) = \exp(-a^2\|\mathbf{h}\|^2) \operatorname{erfi}(a\langle \mathbf{h}, \tilde{\mathbf{x}} \rangle)$. \square

Proof of Proposition 2. We are interested in

$$C_{jk}^{\mathfrak{I}}(\mathbf{h}) = \int_{\mathbb{R}^d} \exp(\mathfrak{i}\langle \mathbf{h}, \mathbf{x} \rangle) \{-\mathfrak{i}\operatorname{sign}(\langle \mathbf{x}, \tilde{\mathbf{x}} \rangle)\} f(\mathbf{x}) d\mathbf{x}$$

where $f(\mathbf{x})$ is the covariance's spectral density. From Proposition 1 of Allard et al. (2022), the spectral density (when it exists) can be represented through the mixture density $g(v)$

$$f(\mathbf{x}) = \int_0^\infty \frac{1}{(2\sqrt{\pi})^d} \exp\left(-\frac{\|\mathbf{x}\|^2}{4v}\right) v^{-\frac{d}{2}} g(v) dv,$$

so that

$$\begin{aligned} C_{jk}^{\mathfrak{I}}(\mathbf{h}) &= \int_{\mathbb{R}^d} \exp(\mathfrak{i}\langle \mathbf{h}, \mathbf{x} \rangle) \{-\mathfrak{i}\operatorname{sign}(\langle \mathbf{x}, \tilde{\mathbf{x}} \rangle)\} \frac{1}{(2\sqrt{\pi})^d} \int_0^\infty \exp\left(-\frac{\|\mathbf{x}\|^2}{4v}\right) v^{-\frac{d}{2}} g(v) dv d\mathbf{x} \\ &= \int_0^\infty \int_{\mathbb{R}^d} \exp(\mathfrak{i}\langle \mathbf{h}, \mathbf{x} \rangle) \{-\mathfrak{i}\operatorname{sign}(\langle \mathbf{x}, \tilde{\mathbf{x}} \rangle)\} \frac{1}{(2\sqrt{\pi})^d} \exp\left(-\frac{\|\mathbf{x}\|^2}{4v}\right) d\mathbf{x} v^{-\frac{d}{2}} g(v) dv \end{aligned}$$

by Fubini's Theorem. The result then follows directly from Proposition 1, as the inner integral satisfies

$$\int_{\mathbb{R}^d} \exp(\mathfrak{i}\langle \mathbf{h}, \mathbf{x} \rangle) \frac{\{-\mathfrak{i}\operatorname{sign}(\langle \mathbf{x}, \tilde{\mathbf{x}} \rangle)\}}{(2\sqrt{\pi})^d} \exp\left(-\frac{\|\mathbf{x}\|^2}{4v}\right) d\mathbf{x} = v^{\frac{d}{2}} \exp(-v\|\mathbf{h}\|^2) \operatorname{erfi}(\sqrt{v}\langle \mathbf{h}, \tilde{\mathbf{x}} \rangle).$$

\square

Proof of Proposition 3. From Allard et al. (2025), the corresponding Cauchy mixing density is Gamma-distributed: $g(v) = a^{-2\alpha}/\{\Gamma(\alpha)\}v^{\alpha-1}\exp(-v/a^2)$, such that

$$C_{jk}^{\mathfrak{R}}(\mathbf{h}) = \frac{1}{(1+a^2\|\mathbf{h}\|^2)^\alpha} = \int_0^\infty e^{-v\|\mathbf{h}\|^2} \frac{a^{-2\alpha}}{\Gamma(\alpha)} v^{\alpha-1} \exp\left(-\frac{v}{a^2}\right) dv.$$

Therefore, we are interested in

$$\begin{aligned} C_{jk}^{\mathfrak{R}}(\mathbf{h}) &= \frac{a^{-2\alpha}}{\Gamma(\alpha)} \int_0^\infty \exp\left\{-v\left(\|\mathbf{h}\|^2 + \frac{1}{a^2}\right)\right\} \operatorname{erfi}(\sqrt{v}\langle \mathbf{h}, \tilde{\mathbf{x}} \rangle) v^{\alpha-1} dv \\ &= \frac{a^{-2\alpha}}{\Gamma(\alpha)} \int_0^\infty \exp\left\{-v\left(\|\mathbf{h}\|^2 + \frac{1}{a^2}\right)\right\} \frac{2\sqrt{v}\langle \mathbf{h}, \tilde{\mathbf{x}} \rangle}{\sqrt{\pi}} {}_1F_1\left(\frac{1}{2}; \frac{3}{2}; v\langle \mathbf{h}, \tilde{\mathbf{x}} \rangle^2\right) v^{\alpha-1} dv, \end{aligned}$$

where the last line follows from 13.6.19 of Abramowitz and Stegun (1948). We consider the change of variables $w = v\langle \mathbf{h}, \tilde{\mathbf{x}} \rangle^2$, so that

$$C_{jk}^{\mathfrak{R}}(\mathbf{h}) = \frac{a^{-2\alpha}}{\Gamma(\alpha)} \frac{2}{\sqrt{\pi}} \langle \mathbf{h}, \tilde{\mathbf{x}} \rangle^{-2\alpha} \int_0^\infty \exp\left\{-w\langle \mathbf{h}, \tilde{\mathbf{x}} \rangle^{-2}\left(\|\mathbf{h}\|^2 + \frac{1}{a^2}\right)\right\} {}_1F_1\left(\frac{1}{2}; \frac{3}{2}; w\right) w^{\alpha-\frac{1}{2}} dw.$$

The result follows from 7.621.4 of Gradshteyn and Ryzhik (2014), which specifies

$$\int_0^\infty w^{\alpha^*-1} e^{-c^*t} {}_1F_1(a^*; b^*; w) dw = (c^*)^{-\alpha^*} \Gamma(\alpha^*) {}_2F_1(a^*, \alpha^*; b^*; 1/c^*).$$

We set $\alpha^* = \alpha + 1/2$, $c^* = \langle \mathbf{h}, \tilde{\mathbf{x}} \rangle^{-2} (\|\mathbf{h}\|^2 + a^{-2})$, $a^* = 1/2$, and $b^* = 3/2$ to get

$$\begin{aligned} C_{jk}^{\mathfrak{I}}(\mathbf{h}) &= \frac{a^{-2\alpha}}{\Gamma(\alpha)} \frac{2}{\sqrt{\pi}} \langle \mathbf{h}, \tilde{\mathbf{x}} \rangle^{-2\alpha} \left(\frac{\|\mathbf{h}\|^2 + a^{-2}}{\langle \mathbf{h}, \tilde{\mathbf{x}} \rangle^2} \right)^{-\alpha - \frac{1}{2}} \Gamma\left(\alpha + \frac{1}{2}\right) \\ &\quad \times {}_2F_1\left(\frac{1}{2}, \frac{1}{2} + \alpha; \frac{3}{2}; \frac{\langle \mathbf{h}, \tilde{\mathbf{x}} \rangle^2}{\|\mathbf{h}\|^2 + a^{-2}}\right) \\ &= \frac{1}{(a^2 \|\mathbf{h}\|^2 + 1)^\alpha} \frac{2}{\sqrt{\pi}} \frac{\Gamma(\alpha + \frac{1}{2})}{\Gamma(\alpha)} \frac{a \langle \mathbf{h}, \tilde{\mathbf{x}} \rangle}{(a^2 \|\mathbf{h}\|^2 + 1)^{\frac{1}{2}}} {}_2F_1\left(\frac{1}{2}, \frac{1}{2} + \alpha; \frac{3}{2}; \frac{a^2 \langle \mathbf{h}, \tilde{\mathbf{x}} \rangle^2}{a^2 \|\mathbf{h}\|^2 + 1}\right). \end{aligned}$$

□

For Propositions A2, 4, and A1, we first introduce and prove Lemma C1. Note that Proposition 4 requires Proposition A2, and Proposition A1 requires Proposition 4, so we follow this order.

Lemma C1 (Spectral density of squared-exponential). Consider a version of the Gneiting class with a squared-exponential spatial covariance:

$$C(\mathbf{h}, u) = \frac{\sigma}{(\gamma(u) + 1)^{\frac{d}{2}}} \exp\left(-\frac{a_s^2 \|\mathbf{h}\|^2}{\gamma(u) + 1}\right). \quad (6)$$

The spectral density of this $C(\mathbf{h}, u)$ in (6) when $\gamma(u) = a_t^2 u^2$ is

$$f^*(\|\mathbf{x}\|, |\eta|) = \frac{a_s}{(2\sqrt{\pi} a_s)^d \sqrt{\pi} a_t \|\mathbf{x}\|} \exp\left(-\frac{\|\mathbf{x}\|^2}{4a_s^2} - \frac{a_s^2 \eta^2}{a_t^2 \|\mathbf{x}\|^2}\right).$$

Furthermore, when $\gamma(u) = a_t |u|$, then the spectral density is

$$f^*(\|\mathbf{x}\|, |\eta|) = \frac{1}{(2\sqrt{\pi} a_s)^d a_t \pi} \exp\left(-\frac{\|\mathbf{x}\|^2}{4a_s^2}\right) \left(\frac{\|\mathbf{x}\|^2}{4a_s^2} + \frac{4a_s^2 \eta^2}{a_t^2 \|\mathbf{x}\|^2}\right)^{-1}.$$

Proof of Lemma C1. First consider the case $\gamma(u) = a_t^2 u^2$. We are interested in the inverse formula

$$\begin{aligned} f^*(\|\mathbf{x}\|, |\eta|) &= (2\pi)^{-d-1} \int_{\mathbb{R}} \int_{\mathbb{R}^d} \exp(-\mathbf{i} \langle \mathbf{h}, \mathbf{x} \rangle - \mathbf{i} \eta u) C(\mathbf{h}, u) d\mathbf{h} du \\ &= (2\pi)^{-d-1} \int_{\mathbb{R}} \int_{\mathbb{R}^d} \frac{\exp(-\mathbf{i} \langle \mathbf{h}, \mathbf{x} \rangle - \mathbf{i} \eta u)}{(a_t^2 u^2 + 1)^{\frac{d}{2}}} \exp\left(-\frac{a_s^2 \|\mathbf{h}\|^2}{a_t^2 u^2 + 1}\right) d\mathbf{h} du \\ &= (2\pi)^{-d-1} \int_{\mathbb{R}} \frac{\exp(-\mathbf{i} \eta u)}{(a_t^2 u^2 + 1)^{\frac{d}{2}}} \int_{\mathbb{R}^d} \exp(-\mathbf{i} \langle \mathbf{h}, \mathbf{x} \rangle) \exp\left(-\frac{a_s^2 \|\mathbf{h}\|^2}{a_t^2 u^2 + 1}\right) d\mathbf{h} du. \end{aligned}$$

From the inverse Fourier transform of the squared-exponential function, we have

$$\begin{aligned}
f^*(\|\mathbf{x}\|, |\eta|) &= (2\pi)^{-d-1} \int_{\mathbb{R}} \frac{\exp(-i\eta u)}{(a_t^2 u^2 + 1)^{\frac{d}{2}}} \exp\left\{-\frac{\|\mathbf{x}\|^2}{4a_s^2} (1 + a_t^2 u^2)\right\} \pi^{\frac{d}{2}} a_s^{-d} (a_t^2 u^2 + 1)^{\frac{d}{2}} du \\
&= \frac{1}{2\pi(2a_s\sqrt{\pi})^d} \int_{\mathbb{R}} \exp(-i\eta u) \exp\left\{-\frac{\|\mathbf{x}\|^2}{4a_s^2} (1 + a_t^2 u^2)\right\} du \\
&= \frac{a_s}{\sqrt{\pi}(2a_s\sqrt{\pi})^d a_t \|\mathbf{x}\|} \exp\left(-\frac{\|\mathbf{x}\|^2}{4a_s^2} - \frac{a_s^2 \eta^2}{a_t^2 \|\mathbf{x}\|^2}\right).
\end{aligned}$$

For the case $\gamma(u) = a_t|u|$, the integration with respect to \mathbf{h} is similar, leaving

$$\begin{aligned}
f^*(\|\mathbf{x}\|, |\eta|) &= \frac{1}{2\pi(2a_s\sqrt{\pi})^d} \int_{\mathbb{R}} \exp(-i\eta u) \exp\left(-\frac{\|\mathbf{x}\|^2}{4a_s^2} (1 + a_t|u|)\right) du \\
&= \frac{1}{2\pi(2a_s\sqrt{\pi})^d} \exp\left(-\frac{\|\mathbf{x}\|^2}{4a_s^2}\right) \int_{\mathbb{R}} \exp(-i\eta u) \exp\left(-\frac{\|\mathbf{x}\|^2}{4a_s^2} a_t|u|\right) du.
\end{aligned}$$

The integral corresponds to the spectral density of the exponential covariance function, resulting in:

$$f^*(\|\mathbf{x}\|, |\eta|) = \frac{1}{2\pi(2a_s\sqrt{\pi})^d} \exp\left(-\frac{\|\mathbf{x}\|^2}{4a_s^2}\right) \frac{2 \frac{\|\mathbf{x}\|^2 a_t}{4a_s^2}}{\frac{\|\mathbf{x}\|^4 a_t^2}{16a_s^4} + \eta^2}.$$

The result then follows from simplifying the fraction. \square

Proof of Proposition A2. The symmetric part follows from Lemma C1. The asymmetric part for $\gamma(u) = a_t^2 u^2$ is

$$\sigma \xi \int_{\mathbb{R}^d} \int_{\mathbb{R}} \exp(i\langle \mathbf{h}, \mathbf{x} \rangle + iu\eta) \operatorname{sign}(\langle \mathbf{x}, \tilde{\mathbf{x}} \rangle) \operatorname{sign}(\eta) f^*(\|\mathbf{x}\|, |\eta|) d\eta d\mathbf{x},$$

with $f^*(\|\mathbf{x}\|, |\eta|)$ as in Lemma C1. This is

$$\begin{aligned}
&\sigma \xi \int_{\mathbb{R}^d} \int_{\mathbb{R}} e^{i\langle \mathbf{h}, \mathbf{x} \rangle + iu\eta} \frac{\operatorname{sign}(\langle \mathbf{x}, \tilde{\mathbf{x}} \rangle) \operatorname{sign}(\eta) a_s}{(2\sqrt{\pi} a_s)^d \sqrt{\pi} a_t \|\mathbf{x}\|} \exp\left(-\frac{\|\mathbf{x}\|^2}{4a_s^2} - \frac{a_s^2 \eta^2}{a_t^2 \|\mathbf{x}\|^2}\right) d\eta d\mathbf{x} \\
&= \sigma \xi \int_{\mathbb{R}^d} \frac{e^{i\langle \mathbf{h}, \mathbf{x} \rangle} \operatorname{sign}(\langle \mathbf{x}, \tilde{\mathbf{x}} \rangle) a_s}{(2\sqrt{\pi} a_s)^d \sqrt{\pi} a_t \|\mathbf{x}\|} \exp\left(-\frac{\|\mathbf{x}\|^2}{4a_s^2}\right) 2 \int_0^\infty \sin(u\eta) \exp\left(-\frac{a_s^2 \eta^2}{a_t^2 \|\mathbf{x}\|^2}\right) d\eta d\mathbf{x},
\end{aligned}$$

as the inner integrand is an odd function of η . The inner integral is related to Dawson's function (3.896.3, Gradshteyn and Ryzhik, 2014): $(1/2) \int_0^\infty \exp(-t^2/4) \sin(zt) dt = D_+(z)$. Applied here with the change of variables $w = 2a_s\eta/(a_t \|\mathbf{x}\|)$, we have

$$\begin{aligned}
2 \int_0^\infty \sin(u\eta) \exp\left(-\frac{a_s^2 \eta^2}{a_t^2 \|\mathbf{x}\|^2}\right) d\eta &= 2 \frac{a_t \|\mathbf{x}\|}{2a_s} \int_0^\infty \sin\left(w \frac{\|\mathbf{x}\|}{2a_s} a_t u\right) \exp\left(-\frac{w^2}{4}\right) dw \\
&= \frac{2a_t \|\mathbf{x}\|}{a_s} D_+\left(\frac{\|\mathbf{x}\|}{2a_s} a_t u\right),
\end{aligned}$$

so that we have

$$\sigma \xi \int_{\mathbb{R}^d} \exp(\mathbf{i}\langle \mathbf{h}, \mathbf{x} \rangle) \frac{2\text{sign}(\langle \mathbf{x}, \tilde{\mathbf{x}} \rangle)}{(2\sqrt{\pi}a_s)^d \sqrt{\pi}} \exp\left(-\frac{\|\mathbf{x}\|^2}{4a_s^2}\right) D_+ \left(\frac{\|\mathbf{x}\|}{2a_s} a_t u\right) d\mathbf{x}.$$

Now, Dawson's function is related to the imaginary error function (7.5.1, [DLMF](#)):

$$D_+ \left(\frac{\|\mathbf{x}\|}{2a_s} a_t u\right) = \frac{\sqrt{\pi}}{2} \exp\left(-\frac{\|\mathbf{x}\|^2}{4a_s^2} a_t^2 u^2\right) \text{erfi}\left(\frac{\|\mathbf{x}\|}{2a_s} a_t u\right).$$

Therefore, we can write the remaining integral as

$$\sigma \xi \int_{\mathbb{R}^d} \exp(\mathbf{i}\langle \mathbf{h}, \mathbf{x} \rangle) \frac{\text{sign}(\langle \mathbf{x}, \tilde{\mathbf{x}} \rangle)}{(2\sqrt{\pi}a_s)^d} \exp\left\{-\frac{\|\mathbf{x}\|^2}{4a_s^2} (a_t^2 u^2 + 1)\right\} \text{erfi}\left(\frac{\|\mathbf{x}\|}{2a_s} a_t u\right) d\mathbf{x}$$

and

$$\sigma \xi \int_{\mathbb{R}^d} \exp(\mathbf{i}\langle \mathbf{h}, \mathbf{x} \rangle) \text{sign}(\langle \mathbf{x}, \tilde{\mathbf{x}} \rangle) f\left(\mathbf{x} \sqrt{a_t^2 u^2 + 1}\right) \text{erfi}\left(\frac{\|\mathbf{x}\|}{2a_s} a_t u\right) d\mathbf{x},$$

where $f(\mathbf{x})$ is the spectral density of the squared-exponential covariance with parameter a_s .

We now consider $\gamma(u) = a_t|u|$. The symmetric half-spectral representation is

$$\sigma \int_{\mathbb{R}^d} \exp(\mathbf{i}\langle \mathbf{h}, \mathbf{x} \rangle) \frac{1}{(2\sqrt{\pi}a_s)^d} \exp\left\{-\frac{\|\mathbf{x}\|^2}{4a_s^2} (a_t|u| + 1)\right\} d\mathbf{x}.$$

The asymmetric representation can be found by applying the Hilbert transform of u , which, for $\exp(-a|u|)$ is demonstrated in [Yarger et al. \(2026\)](#); as well as multiplying a $\text{sign}(\langle \mathbf{x}, \tilde{\mathbf{x}} \rangle)$ term.. This can also be found by relating the result in Lemma [C1](#) to the spectral density of the exponential covariance function. \square

Proof of Proposition 4. The symmetric part follows directly from Lemma [C1](#).

For the asymmetric part when $d = 1$, we use Proposition [A2](#). The integrand is again an odd function, and thus reduces to:

$$\sigma \xi \frac{1}{a_s \sqrt{\pi}} \int_0^\infty \sin(hx) \exp\left\{-\frac{x^2}{4a_s^2} (a_t^2 u^2 + 1)\right\} \text{erfi}\left(\frac{x}{2a_s} a_t u\right) dx.$$

The integral 2.13.1.5 of [Korotkov and Korotkov \(2020\)](#) states that

$$\int_0^\infty \sin(bz) e^{-\gamma z^2} \text{erfi}(cz) dz = \sqrt{\frac{\pi}{4\gamma}} e^{-\frac{b^2}{4\gamma}} \text{erf}\left(\frac{cb}{2\sqrt{\gamma^2 - c^2\gamma}}\right)$$

for $\gamma > c^2$. Setting $c = a_t u / (2a_s)$, $\gamma = (a_t^2 u^2 + 1) / (4a_s^2)$ and $b = h$, the condition $\gamma > c^2$ is

satisfied, and we have that the integral is

$$\begin{aligned} \sigma\xi \frac{1}{a_s\sqrt{\pi}} \sqrt{\frac{\pi}{4} \frac{4a_s^2}{a_t^2u^2+1}} \exp\left(-\frac{a_s^2h^2}{a_t^2u^2+1}\right) \operatorname{erf}\left(\frac{a_tuh}{4a_s\sqrt{\frac{(a_t^2u^2+1)^2}{(4a_s^2)^2} - \frac{a_tu^2(a_t^2u^2+1)}{(4a_s^2)^2}}}\right) \\ = \frac{\sigma\xi}{\sqrt{a_t^2u^2+1}} \exp\left(-\frac{a_s^2h^2}{a_t^2u^2+1}\right) \operatorname{erf}\left(\frac{a_shatu}{\sqrt{a_t^2u^2+1}}\right), \end{aligned}$$

which is the result. \square

Proof of Proposition A1. We mix the asymmetric part of the squared-exponential covariance:

$$\int_0^\infty \frac{\sigma\xi}{\sqrt{a_t^2u^2+1}} \exp\left(-\frac{vh^2}{a_t^2u^2+1}\right) \operatorname{erf}\left(\frac{h\sqrt{v}atu}{\sqrt{a_t^2u^2+1}}\right) g(v) dv,$$

where $g(v)$ is the probability density function of a Gamma random variable:

$$g(v) = \frac{a_s^{-2\alpha}}{\Gamma(\alpha)} v^{\alpha-1} \exp\left(-\frac{v}{a_s^2}\right).$$

This results in the integral

$$\frac{\sigma\xi}{\sqrt{a_t^2u^2+1}} \frac{a_s^{-2\alpha}}{\Gamma(\alpha)} \int_0^\infty \exp\left\{-v\left(\frac{h^2}{a_t^2u^2+1} + \frac{1}{a_s^2}\right)\right\} \operatorname{erf}\left(\sqrt{v} \frac{h a_t u}{\sqrt{a_t^2u^2+1}}\right) v^{\alpha-1} dv.$$

This becomes

$$\begin{aligned} C^*(h, u) &= \frac{\sigma\xi a_s^{-2\alpha}}{\Gamma(\alpha)} \frac{1}{\sqrt{a_t^2u^2+1}} \frac{2}{\sqrt{\pi}} \frac{h a_t u}{\sqrt{a_t^2u^2+1}} \\ &\times \int_0^\infty \exp\left\{-v\left(\frac{h^2}{a_t^2u^2+1} + \frac{1}{a_s^2}\right)\right\} {}_1F_1\left(\frac{1}{2}; \frac{3}{2}; -v \frac{h^2 a_t^2 u^2}{a_t^2 u^2 + 1}\right) v^{\alpha-1} dv, \end{aligned}$$

which follows from 13.6.19 of [Abramowitz and Stegun \(1948\)](#). We consider the change of variables $w = v(h^2 a_t^2 u^2) / (a_t^2 u^2 + 1)$, so that

$$\begin{aligned} C^*(h, u) &= \frac{\sigma\xi a_s^{-2\alpha}}{\Gamma(\alpha)} \frac{\operatorname{sign}(h)\operatorname{sign}(u)}{\sqrt{a_t^2u^2+1}} \frac{2}{\sqrt{\pi}} \left(\frac{a_t^2u^2+1}{h^2 a_t^2 u^2}\right)^\alpha \\ &\times \int_0^\infty \exp\left[-w\left\{\frac{1}{a_t^2u^2} + \frac{a_t^2u^2+1}{(a_shatu)^2}\right\}\right] {}_1F_1\left(\frac{1}{2}; \frac{3}{2}; -w\right) w^{\alpha-1} dw. \end{aligned}$$

The result follows from 7.621.4 of [Gradshteyn and Ryzhik \(2014\)](#), which specifies

$$\int_0^\infty w^{\alpha^*-1} e^{-c^*w} {}_1F_1(a^*; b^*; w) dw = (c^*)^{-\alpha^*} \Gamma(\alpha^*) {}_2F_1(a^*, \alpha^*; b^*; 1/c^*).$$

We set $\alpha^* = \alpha$, $c^* = (a_t^2 u^2)^{-1} + (a_s h a_t u)^{-2} (a_t^2 u^2 + 1)$, $a^* = 1/2$, and $b^* = 3/2$:

$$C^*(h, u) = \frac{\sigma \xi}{\Gamma(\alpha)} \frac{\text{sign}(h)\text{sign}(u)}{\sqrt{a_t^2 u^2 + 1}} \frac{2}{\sqrt{\pi}} \left(\frac{a_t^2 u^2 + 1}{a_s^2 h^2 a_t^2 u^2} \right)^\alpha \left(\frac{1}{a_t^2 u^2} + \frac{a_t^2 u^2 + 1}{(a_s h a_t u)^2} \right)^{-\alpha} \times \Gamma(\alpha) {}_2F_1 \left\{ \frac{1}{2}, \alpha; \frac{3}{2}; - \left(\frac{1}{a_t^2 u^2} + \frac{a_t^2 u^2 + 1}{(a_s h a_t u)^2} \right)^{-1} \right\}.$$

We have

$$\left(\frac{1}{a_t^2 u^2} + \frac{a_t^2 u^2 + 1}{(a_s h a_t u)^2} \right)^{-\alpha} = \left(\frac{a_s^2 h^2 a_t^2 u^2}{a_s^2 h^2 + a_t^2 u^2 + 1} \right)^\alpha,$$

so

$$C^*(h, u) = \sigma \xi \frac{\text{sign}(h)\text{sign}(u)}{\sqrt{a_t^2 u^2 + 1}} \frac{2}{\sqrt{\pi}} \left(\frac{a_t^2 u^2 + 1}{a_s^2 h^2 + a_t^2 u^2 + 1} \right)^\alpha {}_2F_1 \left(\frac{1}{2}, \alpha; \frac{3}{2}; - \frac{a_t^2 u^2 a_s^2 h^2}{a_s^2 h^2 + a_t^2 u^2 + 1} \right).$$

Note that as

$$\frac{a_t u^2 + 1}{a_s^2 h^2 + a_t^2 u^2 + 1} = \left(\frac{a_s^2 h^2}{a_t^2 u^2 + 1} + 1 \right)^{-1},$$

we can write this

$$C^*(h, u) = \sigma \xi \frac{\text{sign}(h)\text{sign}(u)}{\sqrt{a_t^2 u^2 + 1}} \frac{2}{\sqrt{\pi}} \frac{1}{\left(\frac{a_s^2 h^2}{a_t^2 u^2 + 1} + 1 \right)^\alpha} {}_2F_1 \left(\frac{1}{2}, \alpha; \frac{3}{2}; - \frac{a_t^2 u^2 a_s^2 h^2}{a_s^2 h^2 + a_t^2 u^2 + 1} \right).$$

□